Journal of Nonlinear Science (2022) 32:52
https://doi.org/10.1007/s00332-022-09807-8

Journal of Nonlinear Science

Pattern Transformation in Higher-Order Lumps of the Kadomtsev–Petviashvili I Equation

Bo Yang[1] · **Jianke Yang**[2]

Received: 2 October 2021 / Accepted: 25 April 2022

Abstract
Pattern formation in higher-order lumps of the Kadomtsev–Petviashvili I equation at large time is analytically studied. For a broad class of these higher-order lumps, we show that two types of solution patterns appear at large time. The first type of patterns comprises fundamental lumps arranged in triangular shapes, which are described analytically by root structures of the Yablonskii–Vorob'ev polynomials. As time evolves from large negative to large positive, this triangular pattern reverses itself along the x-direction. The second type of patterns comprise fundamental lumps arranged in non-triangular shapes in the outer region, which are described analytically by nonzero-root structures of the Wronskian–Hermit polynomials, together with possible fundamental lumps arranged in triangular shapes in the inner region, which are described analytically by root structures of the Yablonskii–Vorob'ev polynomials. When time evolves from large negative to large positive, the non-triangular pattern in the outer region switches its x and y directions, while the triangular pattern in the inner region, if it arises, reverses its direction along the x-axis. Our predicted patterns at large time are compared to true solutions, and excellent agreement is observed.

Keywords Pattern formation · Lumps · Kadomtsev–Petviashvili I equation

1 Introduction

The Kadomtsev–Petviashvili (KP) equation was derived as a two-dimensional generalization of the Korteweg–de Vries equation for the evolution of weakly nonlinear plasma waves and shallow water waves (Kadomtsev and Petviashvili 1970; Ablowitz

Communicated by Robert Buckingham.

✉ Jianke Yang
jxyang@uvm.edu

[1] School of Mathematics and Statistics, Ningbo University, Ningbo 315211, China

[2] Department of Mathematics and Statistics, University of Vermont, Burlington, VT 05405, USA

Published online: 28 May 2022

and Segur 1979). In the water wave context, this equation reads (Ablowitz and Segur 1979)

$$\left(2f_t + 3ff_x + \left(\frac{1}{3} - T\right) f_{xxx}\right)_x + f_{yy} = 0, \tag{1}$$

where the spatial coordinate x is relative to a certain moving frame, $f(x, y, t)$ represents the water surface elevation, and T is a dimensionless surface tension parameter. If the surface tension is large, i.e., $T > 1/3$, which corresponds to very thin sheets of water, this equation is called KP-I. In this case, rescaling variables by

$$y = \frac{\hat{y}}{\sqrt{3(T - \frac{1}{3})}}, \quad t = -\frac{2\hat{t}}{T - \frac{1}{3}}, \quad f = -2\left(T - \frac{1}{3}\right) u \tag{2}$$

and dropping the hats, this equation becomes

$$(u_t + 6uu_x + u_{xxx})_x - 3u_{yy} = 0. \tag{3}$$

Note that the KP-I equation also arises in other branches of physics, such as nonlinear optics (Pelinovsky et al. 1995) and Bose–Einstein condensates (Barashenkov and Makhankov 1988; Tsuchiya et al. 2008).

The KP-I equation (3) is solvable by the inverse scattering transform (Novikov et al. 1984; Ablowitz and Clarkson 1991). It admits stable fundamental lump solutions that are bounded rational functions decaying in all spatial directions (Petviashvili 1976; Manakov et al. 1977; Satsuma and Ablowitz 1979). These lumps are the counterparts of solitons in the Korteweg–de Vries equation. In the water wave context, these lumps physically correspond to dips on the water surface due to the negative sign in the f scaling above. The KP-I equation also admits a broad class of rational solutions that describe the interactions of these lumps. If individual lumps have distinct asymptotic velocities, then they would pass through each other without change in velocities or phases (Manakov et al. 1977; Satsuma and Ablowitz 1979). But if they have the same asymptotic velocities, they would undergo novel anomalous scattering, where the lumps would separate from each other in new spatial directions that are very different from their original incoming directions (Gorshkov et al. 1993; Ablowitz and Villarroel 1997; Ablowitz et al. 2000). In this article, we are concerned with this latter type of solutions, which we will call higher-order lumps. They are also called multi-pole lumps in the literature (Ablowitz and Villarroel 1997; Ablowitz et al. 2000).

Analytical expressions of higher-order lumps have been derived by a wide variety of methods before (Pelinovsky and Stepanyants 1993; Gorshkov et al. 1993; Ablowitz and Villarroel 1997; Pelinovsky 1998; Ablowitz et al. 2000; Dubard et al. 2010; Dubard and Matveev 2013; Chen et al. 2016; Clarkson and Dowie 2017; Gaillard 2018; Chang 2018; Zhang et al. 2022; Ma 2015). Gorshkov et al. (1993) reported a second-order lump solution that describes the interaction and anomalous scattering of two lumps. Ablowitz and Villarroel (1997); Ablowitz et al. (2000) derived higher-order lumps by the inverse scattering transform and Darboux transformation, and reproduced the

solution in Gorshkov et al. (1993) as a special case. They also showed that when $|t| \to \infty$, these higher-order lumps generically split into a certain number of fundamental lumps, whose relative spatial separations grow in proportion to $|t|^q$, where $\frac{1}{3} \leq q \leq \frac{1}{2}$. In addition, some new lump patterns such as squares at large time were reported. Pelinovsky and Stepanyants (1993) reported a class of higher-order lump solutions that are stationary in a moving frame. Pelinovsky (1998) studied rational solutions of the KP hierarchy and linked them to the dynamics of the Calogero–Moser hierarchy (but his Wronskian-form solutions for KP-I were not made real-valued and thus were not physical solutions). Dubard et al. (2010); Dubard and Matveev (2013) constructed a class of higher-order KP-I lump solutions from higher-order rogue waves of the nonlinear Schrödinger equation, and graphically showed that such second- and third-order lump solutions split into triangles of fundamental lumps when $|t| \to \infty$. Chen et al. (2016) considered a certain class of higher-order lump solutions, and graphically observed that these solutions evolve from a vertical line of fundamental lumps to a horizontal line of fundamental lumps in the (x, y) plane when time goes from negative infinity to infinity. They also predicted the locations of fundamental lumps inside the solution complex at $t = 0$ by roots of certain polynomial equations; but such polynomial equations were not justified. Clarkson and Dowie (2017) derived a second-order lump solution which incorporates the ones in Dubard et al. (2010), Dubard and Matveev (2013), Gorshkov et al. (1993) as special cases. Gaillard (2018) studied a special class of higher-order lump solutions and reported lump patterns such as triangles and pentagons at $t = 0$ when some internal parameters in such solutions get large. Chang (2018) studied the large-time asymptotics of higher-order lumps and showed that, for some special solutions, all lumps are located on a vertical line in the (x, y) plane at large negative time but rotate to a horizontal line at large positive time. Zhang et al. (2022) examined dynamical behaviors of some special higher-order lumps. Ma (2015) derived a fundamental lump solution which contains more free parameters; but that solution can be made equivalent to the original lump solution as reported in Manakov et al. (1977), Satsuma and Ablowitz (1979). We note by passing that non-rational KP-I solutions in the form of a linear periodic chain of lumps, and those that describe the resonant collision between lumps and line solitons, have also been reported recently (Lester et al. 2021; Rao et al. 2021).

In this article, we study pattern formation in higher-order lumps of the KP-I equation (3). This work is motivated by our earlier work on pattern formation of rogue waves in various integrable systems (Yang and Yang 2021a, b), where we showed that universal rogue patterns appear when one of the internal parameters in rogue waves gets large, and those rogue patterns are analytically described by root structures of the Yablonskii–Vorob'ev polynomial hierarchy. For higher-order lumps of the KP-I equation, however, we will focus on their pattern formation at large time rather than at large parameters. In particular, we are interested to know how their patterns at large positive time relate to their patterns at large negative time. For a broad class of higher-order lump solutions, we will show that two types of lump patterns appear at large time. The first type of patterns comprise fundamental lumps arranged in triangular shapes, which are described analytically by root structures of the Yablonskii–Vorob'ev polynomials. As time evolves from large negative to large positive, this triangular pattern reverses itself along the x-direction. The second type of patterns comprise fundamental lumps

arranged in non-triangular shapes in the outer region, which are described analytically by nonzero-root structures of the Wronskian–Hermit polynomials, together with possible fundamental lumps arranged in triangular shapes in the inner region, which are described analytically by root structures of the Yablonskii–Vorob'ev polynomials. When time evolves from large negative to large positive, the non-triangular pattern in the outer region switches its x and y directions, plus some rescaling along each direction, while the triangular pattern in the inner region, if it arises, reverses its direction along the x-axis. These dramatic pattern transformations with the elapse of time are fascinating. We have also compared these predicted patterns with true solutions, and excellent agreement is observed.

This paper is organized as follows. In Sect. 2, we present general higher-order lump solutions in the KP-I equation through Schur polynomials, and introduce Yablonskii–Vorob'ev and Wronskian–Hermit polynomials. In Sect. 3, we present our main analytical results on solution patterns at large time, and explain how these patterns transform from large negative time to large positive time. In Sect. 4, we illustrate our pattern predictions and compare them with true solutions. In Sect. 5, we provide proofs for our analytical results in Sect. 3. The last section summarizes our results, together with some discussions. In the Appendix, a brief derivation of our general higher-order lump solutions in Sect. 2 is given.

2 Preliminaries

The KP equation (3) admits three important invariances. The first one is that it is invariant when $(x, t) \to (-x, -t)$. This invariance is important because it shows that KP-solution patterns are reversible in time (albeit with a sign switch in x). In earlier works (Chen et al. 2016; Chang 2018), the authors showed that certain higher-order KP lumps evolve from a vertical line of fundamental lumps to a horizontal line of fundamental lumps in the (x, y) plane when time goes from negative infinity to infinity. The above invariance indicates that a reverse pattern transformation could also occur, i.e., those higher-order KP lumps can also evolve from a horizontal line to a vertical line when time goes from negative infinity to infinity.

The second invariance of the KP equation (3) is the Galilean invariance (Weiss 1985; Chen et al. 2016), i.e., when

$$(x, y, t) \to (x + 2ky + 12k^2 t,\ y + 12kt,\ t), \tag{4}$$

the KP solution $u(x, y, t)$ remains a solution. Here, k is an arbitrary real constant. This invariance indicates that, if the overall solution complex has a y-direction velocity $12k$, then we can apply this invariance to remove that y-direction velocity. In doing so, the solution pattern in the (x, y) plane would change as well through a linear transformation of shear type. This Galilean invariance is important, because it allows us to remove the overall y-direction velocity in a higher-order lump solution. More will be said on it later in this section.

The third invariance of the KP equation is scaling invariance, i.e., when

$$(x, y, t, u) \to (\alpha x, \alpha^2 y, \alpha^3 t, \alpha^{-2} u), \tag{5}$$

the KP equation remains invariant. Here, α is any nonzero real constant. This invariance is useful since, when combined with the Galilean invariance above, it allows us to normalize the spectral parameter in the KP-lump solutions to be unity without any loss of generality. This we will do in Sec. 3.

2.1 Explicit Expressions of Higher-Order Lumps

In this paper, we consider pattern formation of higher-order lumps in the KP-I equation (3). General higher-order lump solutions have been derived by Ablowitz et al. (2000) through Darboux transformation. Their solutions were given through determinants whose matrix elements involve differential operators with respect to the spectral parameter. For our analysis, those solution expressions are not explicit enough. Thus, we have derived these higher-order lumps again by the bilinear method (Hirota 2004). To present our solutions, we first introduce elementary Schur polynomials $S_k(\boldsymbol{x})$ with $\boldsymbol{x} = (x_1, x_2, \ldots)$, which are defined by the generating function

$$\sum_{n=0}^{\infty} S_n(\boldsymbol{x})\epsilon^n = \exp\left(\sum_{n=1}^{\infty} x_n \epsilon^n\right). \tag{6}$$

More explicitly,

$$S_0(\boldsymbol{x}) = 1, \quad S_1(\boldsymbol{x}) = x_1, \quad S_2(\boldsymbol{x}) = \frac{1}{2}x_1^2 + x_2, \ldots,$$
$$S_n(\boldsymbol{x}) = \sum_{l_1+2l_2+\cdots+ml_m=n} \left(\prod_{j=1}^{m} \frac{x_j^{l_j}}{l_j!}\right).$$

Under these notations, our general higher-order KP-I lumps are given by the following theorem.

Theorem 1 *General N-th-order lumps of the KP-I equation* (3) *are*

$$u_\Lambda(x, y, t) = 2\partial_x^2 \ln \sigma, \tag{7}$$

where

$$\sigma(x, y, t) = \det_{1\le i,j\le N}\left(m_{ij}\right), \tag{8}$$
$$m_{i,j} = \sum_{\nu=0}^{\min(n_i,n_j)} \left(\frac{|p|^2}{(p+p^*)^2}\right)^{\nu} S_{n_i-\nu}\left(\boldsymbol{x}^+ + \nu \boldsymbol{s} + \boldsymbol{a}_i\right)$$

$$\times S_{n_j-v}\left((\boldsymbol{x}^+)^* + v\boldsymbol{s}^* + \boldsymbol{a}_j^*\right), \tag{9}$$

N is an arbitrary positive integer, $\Lambda \equiv (n_1, n_2, \ldots n_N)$ is a vector of arbitrary positive integers, p is an arbitrary non-imaginary complex number, the asterisk '$*$' represents complex conjugation, the vector $\boldsymbol{x}^+ = \left(x_1^+, x_2^+, \ldots\right)$ is defined by

$$x_k^+ = p\frac{1}{k!}x + p^2\frac{2^k}{k!}iy + p^3\frac{3^k}{k!}(-4)t, \tag{10}$$

the vector $\boldsymbol{s} = (s_1, s_2, \ldots)$ is defined through the expansion

$$\ln\left(\frac{1}{\kappa}\left(p + p^*\right)\left(\frac{e^\kappa - 1}{p\,e^\kappa + p^*}\right)\right) = \sum_{j=1}^{\infty} s_j\,\kappa^j, \tag{11}$$

vectors $\boldsymbol{a}_i$ are

$$\boldsymbol{a}_i = \left(a_{i,1}, a_{i,2}, \ldots, a_{i,n_i}\right), \tag{12}$$

and $a_{i,j}$ $(1 \le i \le N, 1 \le j \le n_i)$ are free complex constants.

The proof of this theorem will be given in the Appendix.

Remark 1 In this theorem, positive integers $(n_1, n_2, \ldots n_N)$ do not have to be distinct if their corresponding vectors $\boldsymbol{a}_i$ are different. In such cases, by first rewriting the σ determinant (8) as a larger determinant as was done in Ohta and Yang (2012), then linking Schur polynomials with different $\boldsymbol{a}_i$ vectors in that larger determinant by relations similar to Eq. (167) in Yang and Yang (2021c), and finally applying row operations and parameter redefinitions to the resulting determinant, we can show that this σ determinant (8) with non-distinct integers $(n_1, n_2, \ldots n_N)$ can be reduced to one where the new integers $(\hat{n}_1, \hat{n}_2, \ldots \hat{n}_N)$ become distinct. Thus, in this paper, we will require positive integers $(n_1, n_2, \ldots n_N)$ to be distinct without loss of generality. In this case, we will also arrange them in the ascending order, i.e., $n_1 < n_2 < \cdots < n_N$.

Remark 2 The higher-order lumps in Theorem 1 contain free complex parameters p and $\boldsymbol{a}_i$ $(1 \le i \le N)$, totaling $1 + n_1 + n_2 + \cdots n_N$. However, using techniques similar to that outlined in Remark 1, we can show that $N(N-1)/2$ of those parameters in $\{\boldsymbol{a}_i\}$ can be eliminated. Thus, the number of free complex parameters in these N-th-order lumps can be reduced to $1 + \rho$, where

$$\rho = \sum_{i=1}^{N} n_i - \frac{N(N-1)}{2}. \tag{13}$$

This number of free parameters matches that given in Ablowitz et al. (2000) for solutions produced by Darboux transformation. In fact, from the derivation of Theorem 1 in the Appendix, we can see that our higher-order lumps given in this theorem by the

bilinear method are equivalent to those derived in Ablowitz et al. (2000) by Darboux transformation, except that our expressions are more explicit.

Remark 3 The function $\sigma(x, y, t)$ in (7) is a positive polynomial in x, y and t of degree 2ρ. This will be proved in the Appendix. Thus, the lump solution $u_\Lambda(x, y, t)$ in Theorem 1 is real-valued and nonsingular.

Remark 4 The fundamental lump can be derived by taking $N = 1$ and $n_1 = 1$ in Eq. (8). Through a shift of the (x, y) axes, we can normalize $a_{1,1} = 0$. Then, the resulting $\sigma_1(x, y, t)$ function can be reduced to

$$\begin{aligned}\sigma_1 &= \left|x + 2\mathrm{i}py - 12p^2t\right|^2 + \frac{1}{(p+p^*)^2} \\ &= \left(x - 2p_i\, y - 12(p_r^2 - p_i^2)t\right)^2 + (2p_r(y - 12p_i\, t))^2 + \frac{1}{4p_r^2},\end{aligned} \tag{14}$$

where p_r and p_i are the real and imaginary parts of the spectral parameter p. The corresponding solution $u_1(x, y, t)$ through Eq. (7) moves at x-direction velocity of $12|p|^2$ and y-direction velocity of $12p_i$. By applying the Galilean invariance (4) with $k = p_i$, we can remove the y-direction velocity $12p_i$ and reduce $\sigma_1(x, y, t)$ to

$$\sigma_1 = \left(x - 12p_r^2 t\right)^2 + (2p_r y)^2 + \frac{1}{4p_r^2}. \tag{15}$$

This means that, under Galilean invariance, we can take p in the original fundamental lump to be purely real without loss of generality. Then, by utilizing the scaling invariance (5) with $\alpha = p_r$, we can further normalize p_r in the above σ_1 to be unity. The final simplified fundamental-lump expression is

$$u_1(x, y, t) = 2\partial_x^2 \ln\left((x - 12t)^2 + 4y^2 + \frac{1}{4}\right). \tag{16}$$

This is a moving single lump with peak amplitude 16, which is attained at the spatial location of $(x, y) = (12t, 0)$.

Remark 5 In the general higher-order lump of Theorem 1, the whole solution complex moves at x-direction velocity $12|p|^2$ and y-direction velocity $12p_i$, plus some possible slower motion relative to that moving frame. In this general case, we can also use the Galilean invariance (4) to remove the y-direction velocity $12p_i$ of the complex, i.e., p_i can be made to be zero. In this real-p case, lump solutions in Theorem 1 simplify significantly. First of all, the constant factor in Eq. (9) becomes independent of p. Second, the $\boldsymbol{s}$ vector in the definition (11) becomes independent of p as well. Thus, the dependence of solutions on p only comes in through the vector $\boldsymbol{x}^+$. For real p, we can further use the scaling invariance (5) to normalize p to unity. Thus, without any loss of generality, we can choose p in the higher-order lump solution of Theorem 1 to be equal to one. For this reason, we will set $p = 1$ in the remainder of this paper.

Remark 6 In Pelinovsky and Stepanyants (1993), a class of higher-order lump solutions that are stationary in a moving frame was reported. Those special solutions satisfy the Boussinesq equation. Thus, they are special cases of Boussinesq rogue waves (Yang and Yang 2020). Those stationary higher-order lumps are also special cases of our solutions in Theorem 1 when the index vector $(n_1, n_2, \ldots n_N)$ and internal parameters $\{\boldsymbol{a}_i\}$ are properly chosen. Indeed, rational solutions in Theorem 1 would be stationary if the σ function in (8) satisfies the dimension-reduction condition $\sigma_t - V\sigma_x = 0$, where V is the velocity of the moving frame along the x-direction. In the bilinear derivation of Boussinesq rogue waves (Yang and Yang 2020), one needs to solve the bilinear τ equation of KP-I, together with this τ's dimension reduction condition $\tau_{x_3} - 3\tau_{x_1} = C\tau$, where x_1 is proportional to x, x_3 proportional to t, and C is a constant. Since this τ function turns out to be equal to σ multiplying an exponential of a linear function of x and t (Yang and Yang 2020), we see that τ's dimension reduction condition is equivalent to σ's dimension reduction condition after proper variable scalings. This means that constraints from τ's dimension-reduction condition can be borrowed over and imposed on solutions of Theorem 1 in order to obtain stationary higher-order KP lumps. One of such constraints is on the index vector $(n_1, n_2, \ldots n_N)$, where $n_i = 2i - 1$ must be chosen (Yang and Yang 2020). In addition, internal parameters $\{\boldsymbol{a}_i\}$ also need to be constrained. For a different choice of differential operators than those in Eq. (131) of the Appendix, this parameter constraint was derived in Yang and Yang (2020). For the present choice of differential operators in Eq. (131), this parameter constraint would be more complex. In this case, such a parameter constraint was worked out in Chen et al. (2018) for another integrable system under a different parameterization.

Remark 7 Our bilinear higher-order lumps in Theorem 1 can be related to those derived by the inverse scattering transform (IST) and Darboux transformation (DT) in Ablowitz and Villarroel (1997), Ablowitz et al. (2000). Specifically, our parameter p in Theorem 1 is simply ik_0, where k_0 is a higher-order pole in the spectral k-plane of IST/DT. In this spectral plane, k_0 cannot be real, since the real axis of k separates sectionally meromorphic functions of the scattering problem. This non-real k_0 is equivalent to our condition of p being non-imaginary in Theorem 1.

2.2 Yablonskii–Vorob'ev Polynomials and Wronskian–Hermit Polynomials

We will show in later text that patterns of certain higher-order lump solutions at large time are described by root structures of the Yablonskii–Vorob'ev polynomials and Wronskian–Hermit polynomials. Thus, these polynomials and their root structures will be introduced first.

2.2.1 Yablonskii–Vorob'ev Polynomials and Their Root Structures

Yablonskii–Vorob'ev polynomials arose in rational solutions of the second Painlevé equation (P_{II}) (Yablonskii 1959; Vorob'ev 1965). Later, a determinant expression for these polynomials was found in Kajiwara and Ohta (1996). Let $p_k(z)$ be polynomials defined by

$$\sum_{k=0}^{\infty} p_k(z)\epsilon^k = \exp\left(z\epsilon - \frac{4}{3}\epsilon^3\right). \tag{17}$$

Then, Yablonskii–Vorob'ev polynomials $Q_N(z)$ are given by the $N \times N$ determinant (Kajiwara and Ohta 1996)

$$Q_N(z) = c_N \begin{vmatrix} p_1(z) & p_0(z) & \cdots & p_{2-N}(z) \\ p_3(z) & p_2(z) & \cdots & p_{4-N}(z) \\ \vdots & \vdots & \vdots & \vdots \\ p_{2N-1}(z) & p_{2N-2}(z) & \cdots & p_N(z) \end{vmatrix}, \tag{18}$$

where $c_N = \prod_{j=1}^{N}(2j-1)!!$, and $p_k(z) \equiv 0$ if $k < 0$. This determinant is a Wronskian,

$$Q_N(z) = c_N \operatorname{Wron}\left[p_1(z), p_3(z), \ldots, p_{2N-1}(z)\right], \tag{19}$$

since one can see from Eq. (17) that $p'_{k+1}(z) = p_k(z)$, where the prime represents differentiation. Yablonskii–Vorob'ev polynomials are monic polynomials with integer coefficients (Clarkson and Mansfield 2003), and the first four of them are

$$\begin{aligned} Q_1(z) &= z, \\ Q_2(z) &= z^3 + 4, \\ Q_3(z) &= z^6 + 20z^3 - 80, \\ Q_4(z) &= z(z^9 + 60z^6 + 11200). \end{aligned}$$

Root structures of these polynomials have been studied in Fukutani et al. (2000), Taneda (2000), Clarkson and Mansfield (2003), Buckingham and Miller (2014), Balogh et al. (2016), and the following facts are known.

1. The degree of the $Q_N(z)$ polynomial is $N(N+1)/2$, which can be easily seen from Eq. (18).
2. All roots of $Q_N(z)$ are simple (Fukutani et al. 2000). Thus, $Q_N(z)$ has $N(N+1)/2$ simple roots.
3. Zero is a root of $Q_N(z)$ if and only if $N \equiv 1 \bmod 3$ (Taneda 2000).
4. $Q_N(z)$ can be factorized as $Q_N(z) = z^m f(\zeta)$, where $m = 1$ when $N \equiv 1 \bmod 3$ and $m = 0$ otherwise, $\zeta \equiv z^3$, and $f(\zeta)$ is a polynomial of ζ with integer coefficients and a nonzero constant term (Clarkson and Mansfield 2003). This factorization shows that the root structure of $Q_N(z)$ is invariant under 120°-angle rotation in the complex z plane.
5. Roots of $Q_N(z)$ exhibit a triangular pattern in the complex plane for all $N \geq 2$ (Clarkson and Mansfield 2003; Buckingham and Miller 2014; Balogh et al. 2016). This fact is not surprising given the 120° rotational symmetry of $Q_N(z)$'s root structure mentioned above.
6. Roots of $Q_N(z)$ are also symmetric with respect to the real-z axis, since the coefficients of $Q_N(z)$ are real and thus complex roots appear in conjugate pairs. This

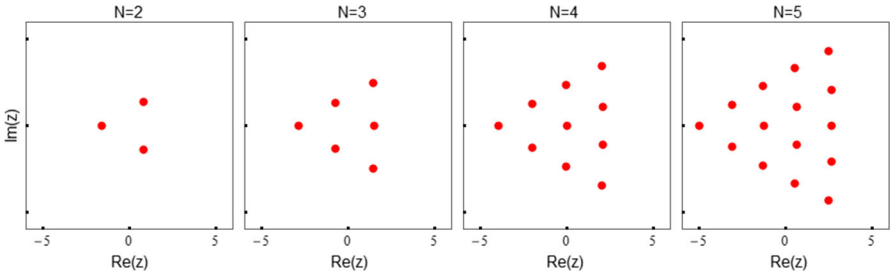

Fig. 1 Root structures of Yablonskii–Vorob'ev polynomials $Q_N(z)$ in the complex z plane for $2 \le N \le 5$

conjugate symmetry, together with the 120° rotational symmetry, implies that one vertex of the triangular root structure of $Q_N(z)$ is on the real-z axis.

Due to importance of these root structures to our work, we reproduce some of them in Fig. 1 for $2 \le N \le 5$.

2.2.2 Wronskian–Hermit Polynomials and Their Root Structures

Next, we introduce Wronskian–Hermit polynomials. Let $q_k(z)$ be polynomials defined by

$$\sum_{k=0}^{\infty} q_k(z)\epsilon^k = \exp\left(z\epsilon + \epsilon^2\right). \tag{20}$$

These $q_k(z)$ polynomials are related to Hermit polynomials through simple variable scalings. Then, for any positive integer N and index vector $\Lambda = (n_1, n_2, \ldots, n_N)$, where $\{n_i\}$ are positive and distinct integers in ascending order, i.e., $n_1 < n_2 < \cdots < n_N$, the Wronskian–Hermite polynomial $W_\Lambda(z)$ is defined as the Wronskian of $q_k(z)$ polynomials

$$W_\Lambda(z) = \mathrm{Wron}\left[q_{n_1}(z), q_{n_2}(z), \ldots, q_{n_N}(z)\right], \tag{21}$$

or equivalently,

$$W_\Lambda(z) = \begin{vmatrix} q_{n_1}(z) & q_{n_1-1}(z) & \cdots & q_{n_1-N+1}(z) \\ q_{n_2}(z) & q_{n_2-1}(z) & \cdots & q_{n_2-N+1}(z) \\ \vdots & \vdots & \vdots & \vdots \\ q_{n_N}(z) & q_{n_N-1}(z) & \cdots & q_{n_N-N+1}(z) \end{vmatrix}, \tag{22}$$

since we can see $q'_{k+1}(z) = q_k(z)$ from the definition (20). In the above determinant, $q_k(z) \equiv 0$ when $k < 0$. These Wronskian–Hermit polynomials appear in monodromy-free Schrödinger operators with quadratically increasing rational potentials (Oblomkov 1999). In addition, if the indices $(n_1, n_2, \ldots, n_N)$ are consecutive,

then these polynomials are called generalized Hermite polynomials which arise in rational solutions of the fourth Painlevé equation (P_{IV}) (Clarkson 2003).

Regarding root structures of Wronskian–Hermite polynomials $W_\Lambda(z)$, we have the following facts.

1. The degree of the polynomial $W_\Lambda(z)$ is equal to ρ, where ρ is given in Eq. (13). This fact can be seen from the definition (22).
2. The multiplicity of the zero root in $W_\Lambda(z)$ is equal to $d(d+1)/2$, where

$$d = k_{\text{odd}} - k_{\text{even}}, \tag{23}$$

and k_{odd}, k_{even} are the numbers of odd and even elements in the index vector $(n_1, n_2, \ldots, n_N)$, respectively. This fact was mentioned in Felder et al. (2012), García-Ferrero and Gómez-Ullate (2015) and proved in Bonneux et al. (2020). If $d(d+1)/2 = 0$, i.e., $d = 0$ or -1, then zero is not a root of $W_\Lambda(z)$.
3. The number of nonzero roots (counting multiplicity) in $W_\Lambda(z)$, which we denote as N_W, is

$$N_W = \rho - \frac{d(d+1)}{2}. \tag{24}$$

4. The polynomial $W_\Lambda(z)$ can be factored as $W_\Lambda(z) = z^{d(d+1)/2} f(\zeta)$, where d is given in Eq. (23), $\zeta \equiv z^2$, and $f(\zeta)$ is a polynomial of ζ with real coefficients and a nonzero constant term (Bonneux et al. 2020).
5. If z_0 is a root of $W_\Lambda(z)$, so are $-z_0$, z_0^* and $-z_0^*$. This quartet root symmetry can be seen from the above factorization of $W_\Lambda(z)$ and the fact that the coefficients of the polynomial $W_\Lambda(z)$ are real. As a consequence of this quartet symmetry, the root structure of $W_\Lambda(z)$ is non-triangular. This is a big difference from Yablonskii–Vorob'ev polynomials, which feature triangular root structures.

In addition, we have the following lemma.

Lemma 1 *The Wronskian–Hermite polynomial $W_\Lambda(z)$ has only zero roots, i.e., $N_W = 0$, if and only if $(n_1, n_2, \ldots, n_N) = (1, 3, 5, \ldots, 2N-1)$.*

Proof Since $k_{\text{odd}} + k_{\text{even}} = N$, we have from Eq. (24) that

$$N_W = \sum_{i=1}^{N} n_i - k_{\text{odd}}^2 - k_{\text{even}}(k_{\text{even}} - 1). \tag{25}$$

Since $\{n_i\}$ are distinct positive integers, their smallest possible values, after reordering, are $\{1, 3, \ldots 2k_{\text{odd}} - 1, 2, 4, \ldots, 2k_{\text{even}}\}$. Thus,

$$\begin{aligned}\sum_{i=1}^{N} n_i &\geq (1 + 3 + \cdots (2k_{\text{odd}} - 1)) + (2 + 4 + \cdots + 2k_{\text{even}}) \\ &= k_{\text{odd}}^2 + k_{\text{even}}(k_{\text{even}} + 1).\end{aligned} \tag{26}$$

Then,

$$N_W \geq 2k_{\text{even}}. \tag{27}$$

For $W_\Lambda(z)$ to have only zero roots, N_W must be zero; so $k_{\text{even}} = 0$, i.e., all numbers in $\{n_i\}$ must be odd. In addition, for the equality in (27) to hold, all these odd and distinct numbers must be the lowest, i.e., $(n_1, n_2, \ldots, n_N) = (1, 3, 5, \ldots, 2N-1)$. This completes the proof. □

This lemma tells us that as long as $\Lambda \neq (1, 3, 5, \ldots, 2N-1)$, the Wronskian–Hermit polynomial $W_\Lambda(z)$ would always have nonzero roots. This result is important to us, as we will show in later text that the presence or absence of nonzero roots in $W_\Lambda(z)$ will have direct consequences on the solution patterns of higher-order lumps.

On roots of Wronskian–Hermite polynomials, beside the above facts, the following conjecture has also been proposed.

Conjecture 1 (Felder et al. 2012). All roots of every Wronskian–Hermite polynomial $W_\Lambda(z)$ are simple, except possibly the zero root.

We will show in later text that the multiplicity of a root in the Wronskian–Hermite polynomial has direct implications on the wave structure of higher-order lumps. Based on this conjecture, $W_\Lambda(z)$ would have N_W nonzero simple roots, where N_W is given in Eq. (24). We have checked this conjecture on a number of examples of $W_\Lambda(z)$, and found it to always hold.

To illustrate root structures of Wronskian–Hermite polynomials, we choose two index vectors

$$\Lambda_1 = (2, 3, 4, 5), \quad \Lambda_2 = (3, 4, 5, 7, 9). \tag{28}$$

For Λ_1, $d = 2 - 2 = 0$, and thus zero is not a root of $W_{\Lambda_1}(z)$ according to the second fact in the earlier text. For Λ_2, $d = 4 - 1 = 3$, and thus zero is a root of multiplicity six in $W_{\Lambda_2}(z)$. Indeed, the full expressions of these two polynomials are

$$W_{\Lambda_1}(z) = \frac{z^8 - 16z^6 + 120z^4 + 720}{2880}, \tag{29}$$

$$W_{\Lambda_2}(z) = -\frac{z^6\left(z^{12} - 12z^{10} + 180z^8 + 672z^6 - 7056z^4 - 181440z^2 - 1270080\right)}{2743372800}, \tag{30}$$

where we can clearly see zero is not a root of $W_{\Lambda_1}(z)$ and is a root of multiplicity six in $W_{\Lambda_2}(z)$. Full root structures of these two polynomials are plotted in Fig. 2. It is seen that for the first polynomial, its root structure is rectangular. (It is not an exact rectangle, but very close; so we will just call it a rectangle in this article.) For the second polynomial, its root structure is quasi-rectangular with a zero root in the center. All nonzero roots in these two polynomials are simple, which is consistent with the earlier conjecture.

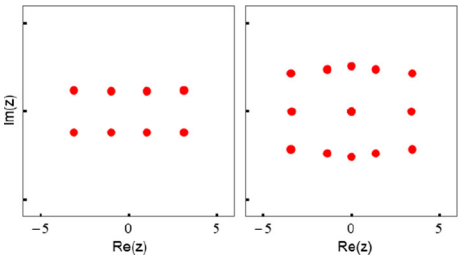

Fig. 2 Root structures of Wronskian–Hermite polynomials $W_{\Lambda_1}(z)$ (left) and $W_{\Lambda_2}(z)$ (right) in the complex plane z, where index vectors Λ_1 and Λ_2 are given in Eq. (28)

For other choices of the index vector Λ, the shape of the root structure could be very different. For example, if we choose $\Lambda = (4, 6, 8, 10, 12)$, then the root structure of $W_\Lambda(z)$ would comprise four arcs, of five roots each, stacked along the imaginary z-axis and surrounding a zero root.

3 Patterns of Higher-Order Lumps at Large Times

In this section, we study patterns of higher-order lumps at large times. In this study, we will set the spectral parameter $p = 1$ without loss of generality (see Remark 5 in the previous section). In this case, the constant factor in Eq. (9) simplifies to $1/4^v$. In addition, the definition (11) of the $\boldsymbol{s}$ vector reduces to

$$\ln\left(\frac{2}{\kappa}\tanh\left(\frac{\kappa}{2}\right)\right) = \sum_{j=1}^{\infty} s_j\,\kappa^j, \tag{31}$$

which is identical to the $\boldsymbol{s}$ vector in the earlier work (Ohta and Yang 2012) on rogue waves of the NLS equation. In particular, all odd-indexed elements s_{odd} of $\boldsymbol{s}$ are zero since the function on the left side of the above equation is even.

It turns out that pattern analysis of lumps depends on whether vector elements $a_{i,j}$ of internal parameters $\{\boldsymbol{a}_i\}$ depend on the i index. In this paper, we only consider the case where $a_{i,j}$ is independent of the i index. In this case, since the length of vector $\boldsymbol{a}_i$ is n_i, and $n_1 < n_2 < \cdots < n_N$, then each $\boldsymbol{a}_i$ for $i < N$ is just a truncation of the longest vector $\boldsymbol{a}_N$. Since every $\boldsymbol{a}_i$ can be extended to the full $\boldsymbol{a}_N$ (or even longer), and the extended parts are dummy parameters which do not appear in the actual solution formulae, by performing this $\boldsymbol{a}_i$ extension, we can say all $\{\boldsymbol{a}_i\}$ vectors are the same in this case and thus denote $\boldsymbol{a}_i = \boldsymbol{a}$. The first element a_1 of $\boldsymbol{a}$ can be further absorbed into (x, y) through a coordinate shift of

$$x + \Re(a_1) \to x, \quad y + \frac{1}{2}\Im(a_1) \to y, \tag{32}$$

where $\Re$ and $\Im$ represent the real and imaginary parts of a complex number. Then, our parameter choices will be

$$\boldsymbol{a}_i = \boldsymbol{a} = (0, a_2, a_3, \ldots). \tag{33}$$

Under these parameters, we have two theorems on patterns of higher-order lumps at large times, depending on whether the index vector Λ is equal to $(1, 3, 5, \ldots, 2N-1)$.

3.1 Large-Time Lump Patterns When $\Lambda = (1, 3, 5, \ldots, 2N-1)$

Our first theorem is for the case where the index vector Λ is equal to $(1, 3, 5, \ldots, 2N-1)$.

Theorem 2 *If the index vector $\Lambda = (1, 3, 5, \ldots, 2N-1)$, then, when $|t| \gg 1$, the N-th-order lump solution $u_\Lambda(x, y, t)$ in Theorem 1 asymptotically separates into $N(N+1)/2$ fundamental lumps $u_1(x - x_0, y - y_0, t)$, where $u_1(x, y, t)$ is given in Eq. (16),*

$$x_0 = \Re(z_0)\,(12t)^{1/3}, \quad y_0 = \frac{\Im(z_0)}{2}(12t)^{1/3}, \tag{34}$$

and z_0 is each of the $N(N+1)/2$ simple roots of the Yablonskii–Vorob'ev polynomial $Q_N(z)$. The peak of each fundamental lump is spatially located at $(x, y) = (12t + x_0, y_0)$. The absolute error of this fundamental-lump approximation is $O(|t|^{-1/3})$ when $z_0 \neq 0$, and $O(t^{-k})$ with k being a certain positive integer when $z_0 = 0$ is a root of $Q_N(z)$. Expressed mathematically, when (x, y) is in the neighborhood of each of these fundamental lumps, i.e., $(x - 12t - x_0)^2 + (y - y_0)^2 = O(1)$, we have the following solution asymptotics for $|t| \gg 1$,

$$u_\Lambda(x, y, t) = \begin{cases} u_1(x - x_0, y - y_0, t) + O\left(|t|^{-1/3}\right), & \text{if } z_0 \neq 0, \\ u_1(x - x_0, y - y_0, t) + O\left(t^{-k}\right), & \text{if } z_0 = 0. \end{cases} \tag{35}$$

When (x, y) is not in the neighborhood of any of these $N(N+1)/2$ fundamental lumps, $u_\Lambda(x, y, t)$ asymptotically approaches zero as $|t| \to \infty$.

The proof of this theorem will be provided in Sect. 5.

This theorem indicates that wave patterns at large times are formed by $N(N+1)/2$ fundamental lumps. Relative to the moving frame of x-direction velocity 12, positions (x_0, y_0) of these fundamental lumps are just a simple linear transformation of the root structure of the Yablonskii–Vorob'ev polynomial $Q_N(z)$, i.e.,

$$\begin{pmatrix} x_0 \\ y_0 \end{pmatrix} = (12t)^{1/3} \begin{pmatrix} 1 & 0 \\ 0 & \frac{1}{2} \end{pmatrix} \begin{pmatrix} \Re(z_0) \\ \Im(z_0) \end{pmatrix}. \tag{36}$$

Since the transformation matrix is diagonal, this transformation is simply a stretching along both horizontal and vertical directions. Recall that the Yablonskii–Vorob'ev root structure is triangular (see Fig. 1). The resulting lump pattern is then triangular as well. When $t \gg 1$, this triangular lump pattern preserves the same orientation of the original triangle of the Yablonskii–Vorob'ev root structure. But when $t \ll -1$, the triangular lump pattern would be oriented opposite of the Yablonskii–Vorob'ev root structure. Indeed, it is easy to see from Eq. (36) that when time changes from large negative to large positive, i.e., from $-t$ to $+t$, their lump positions would be related as

$$\begin{pmatrix} x_0^+ \\ y_0^+ \end{pmatrix} = -\begin{pmatrix} x_0^- \\ y_0^- \end{pmatrix}. \tag{37}$$

Thus, these triangular lump patterns have reversed directions along the x-axis. (The y-direction reversal does not matter since the pattern is symmetric in y.) This x-direction reversal of triangular lump patterns when time changes from large negative to large positive is a dramatic pattern transformation in the KP-I equation. This phenomenon has been graphically reported in Dubard and Matveev (2013) on several low-order solution examples. Here, we established this fact for the general case.

Theorem 2 also indicates that at large time, fundamental lumps in the solution complex separate from each other in proportion to $|t|^{1/3}$. This rate of separation is very slow, relative to the overall (linear) speed 12 of the whole complex.

One more feature of Theorem 2 is that asymptotic positions (x_0, y_0) in Eq. (34) for individual fundamental lumps in the solution complex at large time are independent of the solution's internal parameters $\boldsymbol{a}$. This means that when $|t| \to \infty$, solutions $u_\Lambda(x, y, t)$ with different internal parameters $\boldsymbol{a}$ would approach the same limit solution when $\Lambda = (1, 3, 5, \ldots, 2N-1)$.

3.2 Large-Time Lump Patterns When $\Lambda \neq (1, 3, 5, \ldots, 2N-1)$

When $\Lambda \neq (1, 3, 5, \ldots, 2N-1)$, the Wronskian–Hermite polynomial $W_\Lambda(z)$ has a zero root of multiplicity $d(d+1)/2$, with d given in Eq. (23), as well as nonzero roots that are conjectured to be all simple (see Sect. 2.2.2). Note that the zero root would be absent if $d = 0$ or -1; but nonzero roots always exist. In this case, our results on solution patterns at large time are summarized in the following theorem.

Theorem 3 *Suppose the index vector $\Lambda \neq (1, 3, 5, \ldots, 2N-1)$, and all nonzero roots of the Wronskian–Hermite polynomial $W_\Lambda(z)$ are simple. Then, for $|t| \gg 1$, the following asymptotics for the solution $u_\Lambda(x, y, t)$ holds.*

1. *In the outer region—the region that is $O\left(|t|^{1/2}\right)$ away from the wave center of $(x, y) = (12t, 0)$, or $\sqrt{(x-12t)^2 + y^2} = O\left(|t|^{1/2}\right)$, the higher-order lump $u_\Lambda(x, y, t)$ in Theorem 1 asymptotically separates into N_W fundamental lumps $u_1(x - x_0, y - y_0, t)$, where N_W is given in Eq. (24), $u_1(x, y, t)$ is given in Eq. (16), the lump positions (x_0, y_0) are given by*

$$x_0 = \Re\left(z_0(-12t)^{1/2}\right) - \Re(\Delta), \quad y_0 = \frac{\Im\left(z_0(-12t)^{1/2}\right)}{2} - \frac{\Im(\Delta)}{2}, \tag{38}$$

z_0 is each of the N_W nonzero simple roots of $W_\Lambda(z)$, and $\Delta = \Delta(\Lambda, z_0)$ is an $O(1)$ complex constant given by Eq. (84) in later text. The absolute error of this fundamental-lump approximation is $O(|t|^{-1/2})$. Expressed mathematically, when (x, y) is in the neighborhood of each of these fundamental lumps, i.e., $(x - 12t - x_0)^2 + (y - y_0)^2 = O(1)$, we have the following solution asymptotics

$$u_\Lambda(x, y, t) = u_1(x - x_0, y - y_0, t) + O\left(|t|^{-1/2}\right), \quad |t| \gg 1. \tag{39}$$

2. *If zero is a root of $W_\Lambda(z)$, i.e., $d \neq 0$ and $d \neq -1$, where d is as defined in Eq. (23), then in the inner region—the region that is within $O(|t|^{1/3})$ of the wave center $(x, y) = (12t, 0)$, or $\sqrt{(x-12t)^2+y^2} \leq O\left(|t|^{1/3}\right)$, lies $d(d+1)/2$ fundamental lumps $u_1(x - x_0, y - y_0, t)$, where $u_1(x, y, t)$ is given in Eq. (16), the lump positions (x_0, y_0) are given by*

$$x_0 = \Re(z_0)\,(12t)^{1/3} - \Re(\hat{\Delta}), \quad y_0 = \frac{\Im(z_0)}{2}(12t)^{1/3} - \frac{1}{2}\Im(\hat{\Delta}), \tag{40}$$

z_0 is each of the $d(d+1)/2$ simple roots of the Yablonskii–Vorob'ev polynomial $Q_{\hat{d}}(z)$, with $\hat{d}$ defined as

$$\hat{d} = \begin{cases} d, & \text{when } d \geq 0, \\ |d| - 1, & \text{when } d \leq -1, \end{cases} \tag{41}$$

and $\hat{\Delta} = \hat{\Delta}(\Lambda, z_0)$ is an $O(1)$ complex constant given by Eq. (109) in later text. Notice that $d(d+1)/2 = \hat{d}(\hat{d}+1)/2$. The absolute error of this fundamental-lump approximation is $O(|t|^{-1/3})$ when $z_0 \neq 0$ and $O(t^{-1})$ when zero is a root of $Q_{\hat{d}}(z)$ and $z_0 = 0$. Expressed mathematically, when (x, y) is in the neighborhood of each of these fundamental lumps, i.e., $(x - 12t - x_0)^2 + (y - y_0)^2 = O(1)$, with (x_0, y_0) given in (40), we have the following solution asymptotics for $|t| \gg 1$,

$$u_\Lambda(x, y, t) = \begin{cases} u_1(x - x_0,\ y - y_0, t) + O\left(|t|^{-1/3}\right), & \text{if } z_0 \neq 0, \\ u_1(x - x_0,\ y - y_0, t) + O\left(t^{-1}\right), & \text{if } z_0 = 0. \end{cases} \tag{42}$$

3. *When (x, y) is not in the neighborhood of any of the above fundamental lumps specified by Eqs. (38) and (40) in the (x, y) plane, including when (x, y) is between the outer and inner regions, $u_\Lambda(x, y, t)$ asymptotically approaches zero as $|t| \to \infty$.*

Remark 8 In this theorem, we assumed all nonzero roots of $W_\Lambda(z)$ simple, which is true for all examples we tested, such as the two in Eqs. (29)–(30). In view of Conjecture 1 in the previous section, this assumption is expected to hold in all cases. If this conjecture is false, i.e., some nonzero roots of $W_\Lambda(z)$ are not simple, then this theorem for the outer region, i.e., Eqs. (38)–(39), would still hold, but only for nonzero simple roots z_0 of $W_\Lambda(z)$.

Remark 9 If the index vector $\Lambda = (1, 3, 5, \ldots, 2N-1)$, the above theorem is still valid. In this case, the Wronskian–Hermite polynomial $W_\Lambda(z)$ does not have any nonzero roots (see Lemma 1 in Sect. 2.2.2). Thus, there are no outer regions here. In addition, $\hat{\Delta} = 0$, since we can readily show $\alpha_{k_{odd}} = \beta_{k_{\text{even}}} = 0$ in the expression (109) of $\hat{\Delta}$. Furthermore, $d = N$. Thus, the inner-region lump predictions (40)–(42) reduce to that given in Theorem 2. This means that Theorem 2 is a special case of Theorem 3 if we let Λ arbitrary in the latter theorem. The reason we still write Theorem 2 as a separate theorem is that both the results and their proofs in that special case are indeed much simpler.

Now, we explain what Theorem 3 says regarding solution patterns at large times when $\Lambda \neq (1, 3, 5, \ldots, 2N-1)$. In this case, Theorem 3 indicates that the whole wave field is generically split up into two regions featuring different patterns.

1. In the outer region, the region that is $O(|t|^{1/2})$ away from the wave center $(x, y) = (12t, 0)$, the wave field at large time comprises N_W fundamental lumps. Relative to the moving frame of x-direction velocity 12, positions (x_0, y_0) of these fundamental lumps, to the leading order of large time, are just a linear transformation of $W_\Lambda(z)$'s nonzero-root structure. The reader is reminded from Sect. 2.2.2 that when $\Lambda \neq (1, 3, 5, \ldots, 2N-1)$, nonzero roots of $W_\Lambda(z)$ always exist, and their shape in the z-plane is non-triangular. When t is large negative, these fundamental-lump positions to the leading order are

$$\begin{pmatrix} x_0^- \\ y_0^- \end{pmatrix} = (12|t|)^{1/2} \begin{pmatrix} 1 & 0 \\ 0 & \frac{1}{2} \end{pmatrix} \begin{pmatrix} \Re(z_0) \\ \Im(z_0) \end{pmatrix}, \tag{43}$$

where z_0 is any nonzero root of $W_\Lambda(z)$. However, when t is large positive, these lump positions become

$$\begin{pmatrix} x_0^+ \\ y_0^+ \end{pmatrix} = (12|t|)^{1/2} \begin{pmatrix} 0 & -1 \\ \frac{1}{2} & 0 \end{pmatrix} \begin{pmatrix} \Re(z_0) \\ \Im(z_0) \end{pmatrix}. \tag{44}$$

In the former case, the wave pattern formed by these fundamental lumps is simply a stretching of the Wronskian–Hermite nonzero-root structure along both horizontal and vertical directions. But in the latter case, on top of this stretching, the horizontal and vertical directions are also swapped. In both cases, the resulting wave patterns from transformations (43)–(44) are non-triangular since the root structure of $W_\Lambda(z)$ is non-triangular.

From the above two transformations, we see that fundamental lumps at large negative time $-t$ and large positive time $+t$ in the outer region are related as

$$\begin{pmatrix} x_0^+ \\ y_0^+ \end{pmatrix} = \begin{pmatrix} 0 & -2 \\ \frac{1}{2} & 0 \end{pmatrix} \begin{pmatrix} x_0^- \\ y_0^- \end{pmatrix}. \tag{45}$$

Thus, when time goes from large negative to large positive, outer-region lump patterns in the (x, y) plane have swapped horizontal and vertical directions. In addition, stretching of different amounts has also occurred along the two directions. This swapping of horizontal and vertical directions is another type of dramatic pattern transformation, and it is very different from the triangular x-direction reversal that occurs when $\Lambda = (1, 3, 5, \ldots, 2N-1)$. For certain single-line patterns of fundamental lumps, a change from a vertical line to a horizontal line in the (x, y) plane has been graphically reported in Chen et al. (2016) and analytically explained in Chang (2018). Here, we proved this fact for the general case, where patterns of fundamental lumps based on Wronskian–Hermite root structures can be arbitrary, not just lines (see the next section for examples).

In this outer region, fundamental lumps at large time separate from each other in

proportion to $|t|^{1/2}$. This is another big difference between the present solutions and those with $\Lambda = (1, 3, 5, \ldots, 2N-1)$ in the previous subsection, where lumps separate in proportion to $|t|^{1/3}$ instead.

2. In the inner region, the region that is within $O(|t|^{1/3})$ of the wave center $(x, y) = (12t, 0)$, if $d \neq 0$ and -1, then the solution $u_\Lambda(x, y, t)$ at large time would comprise $d(d+1)/2$ fundamental lumps, where d is defined in Eq. (23). Relative to the moving frame of x-direction velocity 12, positions (x_0, y_0) of these fundamental lumps, to the leading order of large time, are just a linear transformation of $Q_{\hat{d}}(z)$'s root structure, i.e.,

$$\begin{pmatrix} x_0 \\ y_0 \end{pmatrix} = (12t)^{1/3} \begin{pmatrix} 1 & 0 \\ 0 & \frac{1}{2} \end{pmatrix} \begin{pmatrix} \Re(z_0) \\ \Im(z_0) \end{pmatrix}, \tag{46}$$

where $\hat{d}$ is defined in Eq. (41), and z_0 is each of the $d(d+1)/2$ simple roots of $Q_{\hat{d}}(z)$. The reader is reminded that $\hat{d}(\hat{d}+1)/2 = d(d+1)/2$. This lump-position formula in the inner region is very similar to (36) of the $\Lambda = (1, 3, 5, \ldots, 2N-1)$ case. Thus, the pattern of these $d(d+1)/2$ fundamental lumps in the inner region at large time is a simple stretching of $Q_{\hat{d}}(z)$'s root structure, and the resulting pattern is triangular if $\hat{d} > 1$. In addition, as time evolves from large negative to large positive, these triangular lump patterns would reverse direction along the x-axis. Furthermore, fundamental lumps in this inner region separate from each other in proportion to $|t|^{1/3}$ at large time, similar to the $\Lambda = (1, 3, 5, \ldots, 2N-1)$ case in Theorem 2. If $\hat{d} = 0$, i.e., $d = 0$ or -1, this inner region would be absent.

The above results reveal that the pattern of the solution $u_\Lambda(x, y, t)$ for $\Lambda \neq (1, 3, 5, \ldots, 2N-1)$ at large time is richer, with the outer region exhibiting the non-triangular shape of the stretched nonzero-root structure of the Wronskian–Hermite polynomial $W_\Lambda(z)$, and with the inner region exhibiting the triangular shape of the stretched root structure of the Yablonskii–Vorob'ev polynomial $Q_{\hat{d}}(z)$. As time changes from large negative to large positive, the outer pattern swaps horizontal and vertical directions, while the inner pattern reverses the horizontal direction. These different types of pattern transformations in the outer and inner regions of the same solution are fascinating. When $\Lambda \neq (1, 3, 5, \ldots, 2N-1)$, the outer pattern is always present since $W_\Lambda(z)$ always has nonzero roots, but the inner pattern is present only when $d \neq 0$ and -1 and absent otherwise. When $\Lambda = (1, 3, 5, \ldots, 2N-1)$, the outer pattern disappears, and the inner-region prediction in Theorem 3 reduces to the results in Theorem 2 (see Remark 9).

Similar to Theorem 2, Theorem 3 also says that asymptotic positions (x_0, y_0) in Eqs. (38) and (40) for individual fundamental lumps in the outer and inner regions of the solution complex at large time are independent of the solution's internal parameters $\boldsymbol{a}$. Thus, when $|t| \to \infty$, solutions $u_\Lambda(x, y, t)$ with different internal parameters $\boldsymbol{a}$ would approach the same limit solution as well when $\Lambda \neq (1, 3, 5, \ldots, 2N-1)$.

In earlier work (Ablowitz et al. 2000), it was reported that at large time, fundamental lumps in the higher-order lump complex separate from each other in proportion to $|t|^q$, where $\frac{1}{3} \leq q \leq \frac{1}{2}$. Our results in Theorems 2 and 3 indicate that this q value can only be $1/3$ or $1/2$, nothing in between.

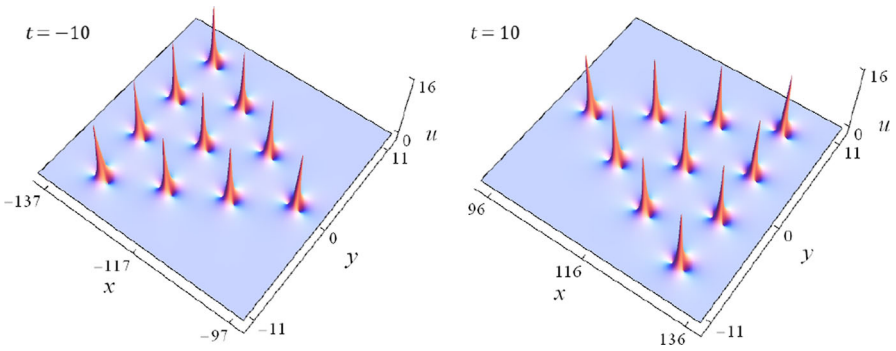

Fig. 3 Predicted solutions $u_\Lambda(x, y, t)$ with $\Lambda = (1, 3, 5, 7)$ at time values of $t = -10$ (left) and $t = 10$ (right)

4 Comparison Between True Lump Patterns and Analytical Predictions

In this section, we compare our analytical predictions of lump patterns with true solutions.

4.1 Pattern Transformation When $\Lambda = (1, 3, 5, \ldots, 2N-1)$

First, we do the comparison when $\Lambda = (1, 3, 5, \ldots, 2N-1)$, where a triangular pattern of lumps at large time is predicted. To be specific, we take $N = 4$; so $\Lambda = (1, 3, 5, 7)$. Root structure of the corresponding Yablonskii–Vorob'ev polynomial $Q_4(z)$ is shown in Fig. 1. Using those roots and formulae (34), predicted solutions from Theorem 2 at large times $t = -10$ and 10 are plotted in Fig. 3.

Now, we compare these predicted solutions with true ones. In the true solution $u_\Lambda(x, y, t)$, we select its internal parameters as $\boldsymbol{a} = (0, 0, 0, 0, 0, 0, 0)$. Then, evolutions of this true solution, at six time values of $t = -10,\ -1,\ 0,\ 0.2,\ 1$ and 10, are plotted in Fig. 4. When comparing these true solutions at large times $t = \pm 10$ to those predicted in Fig. 3, they clearly match each other to the eye. Indeed, the true solutions at $t = \pm 10$ exhibit a triangular pattern, and the triangular pattern at $t = 10$ is a x-direction reversal of the triangular pattern at $t = -10$ (relative to a frame moving in the x-direction with velocity 12), just as what the theory predicted.

We have also performed a quantitative comparison between predicted and true solutions at various time values in order to verify the error decay rate given in Eq. (35) of Theorem 2. For this purpose, the predicted and true solutions are shown on top of each other at two time values of $t = 2$ and 20 in the left and middle panels of Fig. 5, respectively, where the predicted lump locations are marked by dashed circles. We can see that the prediction at $t = 20$ is more accurate than at $t = 2$, meaning that the error of prediction decreases as $|t|$ increases. To determine at what rate this error decreases, we plot in the right panel of Fig. 5 the error of prediction versus time for the top lump marked by a white arrow in the mid-panel. Here, the error is measured as the distance between peak locations of true and predicted lumps. For this chosen

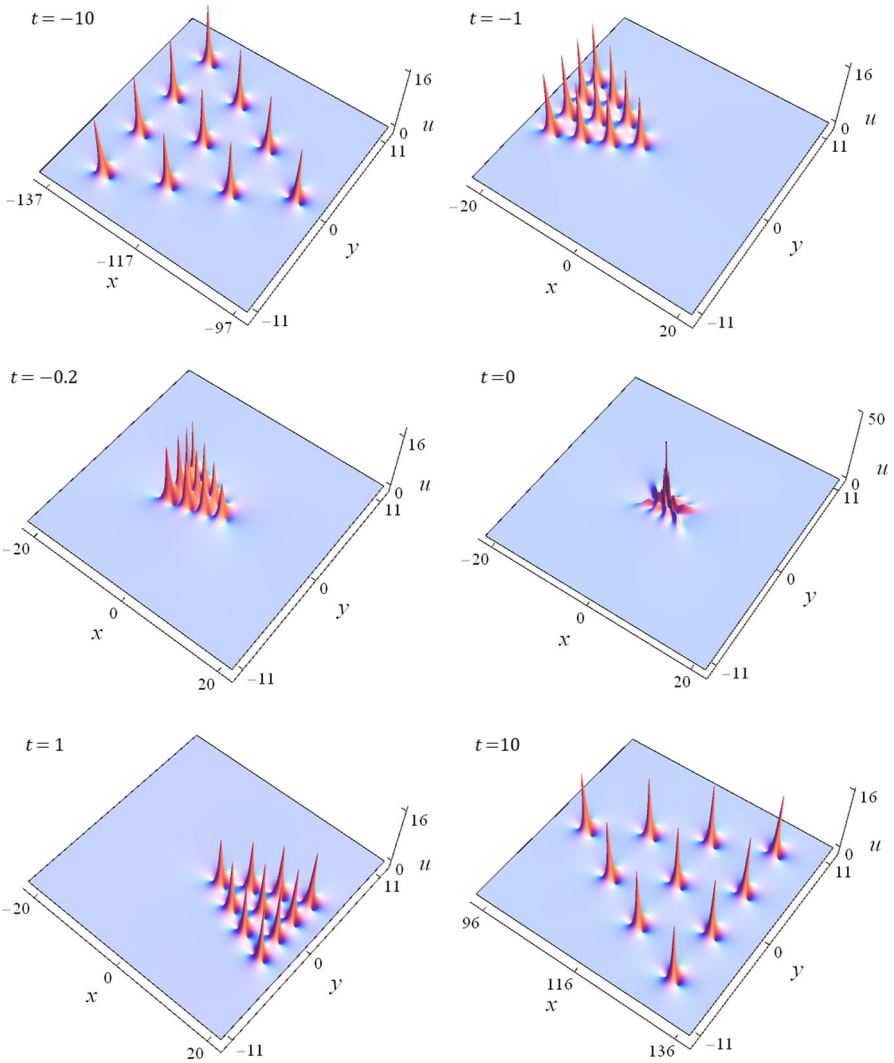

Fig. 4 True solution $u_\Lambda(x, y, t)$ with $\Lambda = (1, 3, 5, 7)$ and $\boldsymbol{a} = (0, 0, 0, 0, 0, 0, 0)$ at various time values shown inside the panels. In all panels, lengths of the x intervals are the same, but the intervals are changing since the wave ensemble is moving along the x direction at the speed of 12

lump, $z_0 \neq 0$. Thus, the predicted error decay rate from Eq. (35) is $O(|t|^{-1/3})$. The true error decay from this panel clearly shows that the decay rate is indeed $O(|t|^{-1/3})$, which confirms the theory. We have also performed error analysis for the center lump, where $z_0 = 0$, found that the difference between the predicted lump and the true one is $O(t^{-2})$, which agrees with Eq. (35) where $k = 2$ for the $z_0 = 0$ case. Thus, our asymptotic theory in Theorem 2 is fully confirmed by this example of $\Lambda = (1, 3, 5, 7)$.

In addition to large times, Fig. 4 also displays the true solution $u_\Lambda(x, y, t)$ at intermediate times, where our asymptotic theory does not apply. These intermediate panels shed light on how the dramatic x-direction reversal of triangular patterns takes

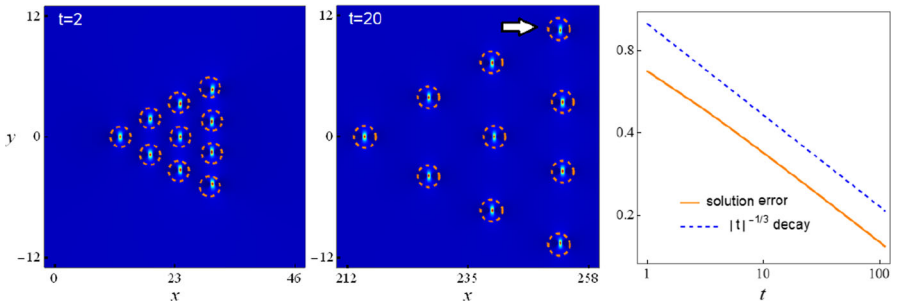

Fig. 5 Verification of the error decay rate in Eq. (35) of Theorem 2 for the example of Fig. 4. The left and middle panels show density plots of true solutions, together with predicted locations of fundamental lumps marked by dashed circles, at $t = 2$ and 20, respectively. The right panel shows the decay rate of error versus t for the lump marked by a while arrow in mid-panel (the $|t|^{-1/3}$ decay is also plotted for comparison)

place as time changes from large negative to large positive. We see that in this solution, as time increases from -10 to 10, the triangle of fundamental lumps first approach each other and shrink in size, then coalesce at $t = 0$ and form a single lump of extreme height that is ten times that of original fundamental lumps, and then separate into a triangle of fundamental lumps again but with reversed x-direction. This transformation process is fascinating.

How will this $u_\Lambda(x, y, t)$ solution evolve if its internal parameters $\boldsymbol{a}$ are different from $(0, 0, 0, 0, 0, 0, 0)$? Theorem 2 tells us that for any other parameter vector $\boldsymbol{a}$, the $u_\Lambda(x, y, t)$ solution would approach the same asymptotic triangular state as that shown in Fig. 4 when time is large (see the last paragraph of Sect. 3.1). To verify this prediction, we have numerically plotted the $u_\Lambda(x, y, t)$ solutions at several other nonzero $\boldsymbol{a}$ values, and found that these solutions indeed approach the u solution of all-zero $\boldsymbol{a}$ when time approaches infinity. At intermediate times, however, this $u_\Lambda(x, y, t)$ solution would definitely depend on the choice of the $\boldsymbol{a}$ values. For instance, by suitably choosing nonzero $\boldsymbol{a}$ values, we can get $u_\Lambda(x, y, t)$ solutions whose graphs at $t = 0$ exhibit very different patterns such as a pentagon or a heptagon—a phenomenon that has been reported in Gaillard (2018). Thus, although these $u_\Lambda(x, y, t)$ solutions with different $\boldsymbol{a}$ values approach the same triangular patterns at large time, how this triangular pattern at large negative time transforms to its x-reversed pattern at large positive time is a process that strongly depends on the choice of the internal $\boldsymbol{a}$ values.

4.2 Pattern Transformation When $\Lambda \neq (1, 3, 5, \ldots, 2N - 1)$

Next, we perform comparison when $\Lambda \neq (1, 3, 5, \ldots, 2N - 1)$, where the solution pattern at large time is dictated by the nonzero-root structure of the Wronskian–Hermit polynomial $W_\Lambda(z)$ in the outer region, and by the root structure of the Yablonskii–Vorob'ev polynomial $Q_{\hat{d}}(z)$ in the inner region (if $\hat{d} > 0$). Since this inner region can be present or absent depending on the d value [see Eq. (23)], we will present two examples, one for each case.

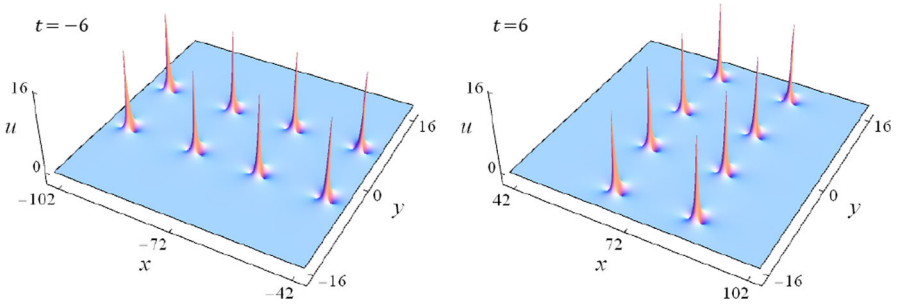

Fig. 6 Predicted solutions $u_\Lambda(x, y, t)$ with $\Lambda = (2, 3, 4, 5)$ at time values of $t = -6$ (left) and $t = 6$ (right)

4.2.1 The First Example

Our first example is $N = 4$ and $\Lambda = (2, 3, 4, 5)$. In this case, $d = 0$, and thus zero is not a root of $W_\Lambda(z)$ and the inner region is absent. Root structure of the corresponding Wronskian–Hermit polynomial is shown in Fig. 2 (left panel). It was seen that this $W_\Lambda(z)$ admits eight simple nonzero roots z_0 which form a rectangle pattern. For the eight roots of $W_\Lambda(z)$ in the left panel of Fig. 2, from the left to right, the corresponding $\Delta(\Lambda, z_0)$ values in the position prediction (38) can be computed from the formula (84) as

$$\begin{aligned}\Delta(\Lambda, z_0) \approx &-3.0902 \pm 0.3139\mathrm{i},\ -1.6155 \pm 0.0980\mathrm{i},\\ &-1.6155 \pm 0.0980\mathrm{i},\ -3.0902 \pm 0.3139\mathrm{i}\end{aligned} \tag{47}$$

when $t > 0$, and

$$\begin{aligned}\Delta(\Lambda, z_0) \approx &-0.2743 \pm 0.3139\mathrm{i}, -1.0199 \pm 0.0980\mathrm{i},\\ &-1.0199 \pm 0.0980\mathrm{i}, -0.2743 \pm 0.3139\mathrm{i}\end{aligned} \tag{48}$$

when $t < 0$. Using these z_0 roots and Δ values, predicted lump patterns from Eq. (38) of Theorem 3 at large times $t = -6$ and 6 are plotted in Fig. 6. The predicted patterns contain eight fundamental lumps which also form an approximate rectangle in the (x, y) plane. (These approximate rectangles are further explained in Fig. 8.) At $t = -6$, this lump pattern is roughly a stretching of the Wronskian–Hermit root structure. But at $t = 6$, this lump pattern has swapped its x and y directions and changed from its original x-direction orientation to the new y-direction orientation.

To confirm these asymptotic predictions, we plot in Fig. 7 the corresponding true solution $u_\Lambda(x, y, t)$ at six time values of $t = -6, -2, -0.5, 0, 2$ and 6. In this true solution, we have selected its internal parameters as $\boldsymbol{a} = (0, 0, 0, 0, 800)$. Here, we intentionally chose a large a_5 value in order to test our asymptotic theory for large $\boldsymbol{a}$ parameters. As given in Sect. 5.3, our large-time asymptotics for the outer region in Theorem 3 will remain valid when some a_k parameters in $\boldsymbol{a}$ are large, as long as $|t|$ is adequately large. Here, the large parameter is $a_5 = 800$. According to Eq. (122) of

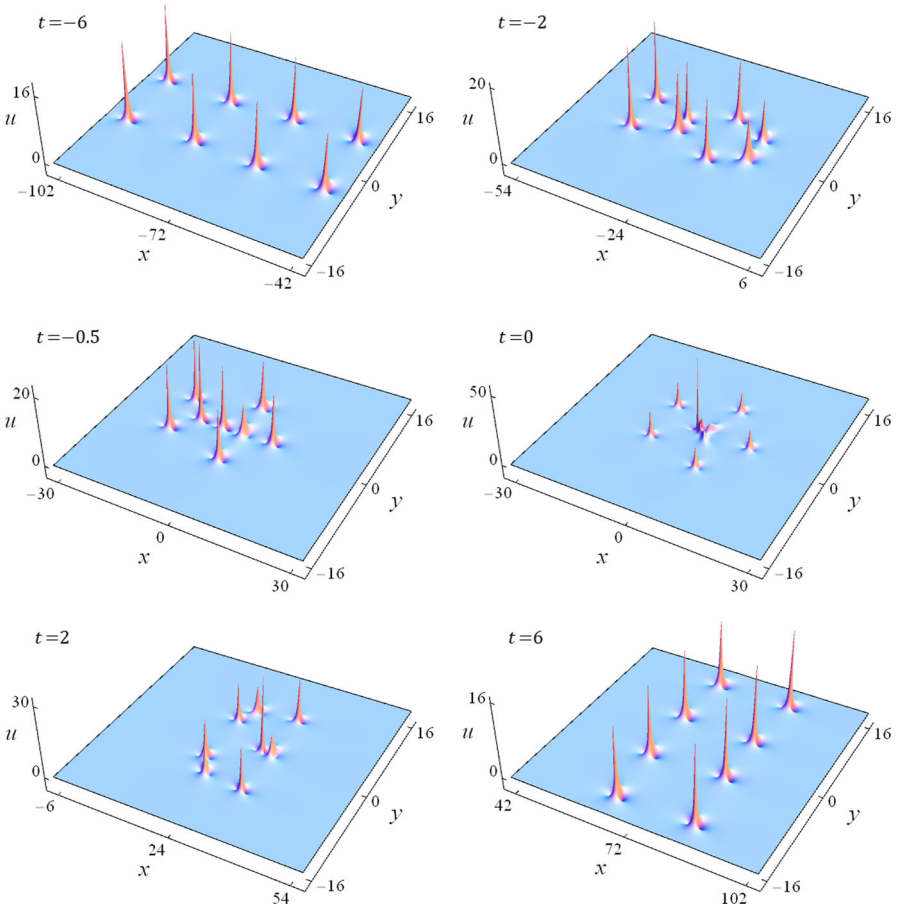

Fig. 7 True solutions $u_\Lambda(x, y, t)$ with $\Lambda = (2, 3, 4, 5)$ and $\boldsymbol{a} = (0, 0, 0, 0, 800)$, at various times whose values are shown inside the panels

Sect. 5.3, our outer-region asymptotics would be valid when $|t| \geq O\left(|a_5|^{2/3}/12\right) \approx O(7)$. Thus, time does not need to be very large for our theory to hold. Indeed, when we compare true solutions at $t = \pm 6$ with predictions in Fig. 6, we can see that they visually already agree well with each other despite the large a_5. In particular, the true solutions indeed comprise eight fundamental lumps forming an approximate rectangle, and their orientations have changed from the x-direction to the y-direction as time changes from -6 to 6, exactly as our asymptotic theory in Fig. 6 has predicted.

To verify the error decay rate given in Eq. (39) of Theorem 3 for predictions in the outer region, we further perform a quantitative comparison for different times. At two time values of $t = 3$ and 20, we first show predicted lump locations as dashed circles in the left and middle panels of Fig. 8, respectively. Notice that these predicted patterns, comprising eight fundamental lumps, are slightly curvy. (This curvature is also present in Fig. 6 but was hard to see due to the way of our plotting.) The reason for this curvy

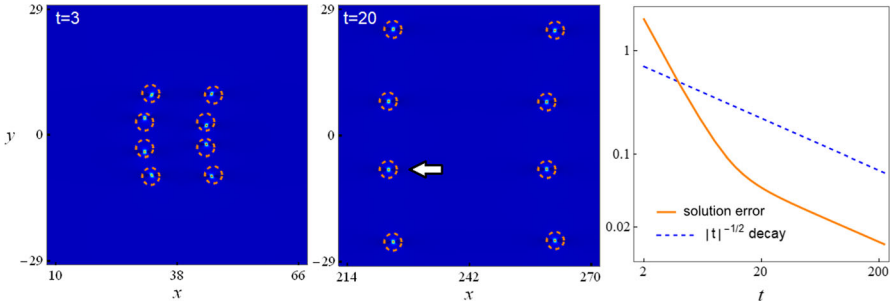

Fig. 8 Verification of the outer-region's error decay rate in Eq. (39) of Theorem 3 for the example of Fig. 7. The left and middle panels show density plots of true solutions, together with predicted locations of fundamental lumps marked by dashed circles, at $t = 3$ and 20, respectively. The right panel shows the decay rate of error versus t for the lump marked by a while arrow in mid-panel (the $|t|^{-1/2}$ decay is also plotted for comparison)

shape is due to the different Δ values in Eq. (47) for these eight lumps, starting from the bottom up, which induce different amounts of $O(1)$ position shifts to the leading-order lump positions in Eq. (38). While the leading-order terms in (38) produce a rectangular lump pattern corresponding to the root structure in Fig. 2 (left panel), different $O(1)$ shifts to these lumps out of different Δ values cause this rectangular shape to bend and exhibit curvature. But this curvature will gradually disappear as $|t|$ increases, since the leading-order term in the position formula (38) will become more dominant. Indeed, Fig. 8 shows that the curvature at $t = 20$ is much weaker than at $t = 3$.

Now, we plot true lump solutions at these time values, as density graphs, on top of these predicted solutions. By visually comparing them, we see that true lump patterns are also slightly curvy, consistent with the prediction. In addition, predicted lump positions at $t = 20$ are more accurate than at $t = 3$, meaning that the error decreases with time. To determine the error decay rate, we plot in the right panel of Fig. 8 the error of prediction versus time for the lump marked by a white arrow in the mid-panel. This error panel shows that the error's decay rate is $O(|t|^{-1/2})$ at large time, which confirms the prediction in Eq. (39). In addition, this $O(|t|^{-1/2})$ decay is reached for time larger than roughly 20, which is consistent with our estimate of $|t| \geq O(7)$ earlier. Importantly, this time value of 20 is much less than the a_5 value of 800, confirming the fact that the validity of our asymptotics often does not require $|t|$ to be much larger than internal parameters $|a_k|$. To fully confirm our estimate of $|t| \geq O\left(|a_5|^{2/3}/12\right)$ in Eq. (122) for the validity of our asymptotic theory, we have also increased a_5 above 800 and re-plotted the error decay curve versus time. We find that the time value above which the $O(|t|^{-1/2})$ decay is reached is indeed proportional to $|a_5|^{2/3}/12$. Thus, our asymptotic theory in Theorem 3 for outer lumps is fully verified for $\Lambda = (2, 3, 4, 5)$.

By inspecting Fig. 7, we can also see how this dramatic rectangular-pattern reorientation takes place as time increases. First, these eight fundamental lumps of rectangular shape with x-direction orientation get closer to each other and rearrange their shapes. At $t = 0$, the solution has evolved into a pentagon of five fundamental lumps surrounding a higher-peak lump near the center. Afterwards, this pentagon structure further adjusts its shape in significant ways, until eight new fundamental lumps emerge as a

rectangular with y-direction orientation in the end. Again, this transformation process is amazing.

4.2.2 The Second Example

Our second example is $N = 5$ and $\Lambda = (3, 4, 5, 7, 9)$. In this case, $d = 3$, and thus zero is a root of multiplicity six in $W_\Lambda(z)$, and the inner region is present. Root structure of the corresponding Wronskian–Hermit polynomial is shown in Fig. 2 (right panel). It is seen that this $W_\Lambda(z)$ admits 12 simple nonzero roots which form a quasi-rectangular shape, plus the zero root of multiplicity six at the center of the quasi-rectangle. Using formula (84), we find that for these twelve nonzero roots z_0 of $W_\Lambda(z)$ in the right panel of Fig. 2, from the left to right,

$$\begin{aligned}\Delta(\Lambda, z_0) \approx & -3.9717 \pm 0.4315\mathrm{i}, -3.6158, -2.0475 \pm 1.0544\mathrm{i}, -0.6449, \\ & -0.6449, -2.0475 \pm 1.0544\mathrm{i}, -3.6158, -3.9717 \pm 0.4315\mathrm{i}\end{aligned}$$

when $t > 0$, and

$$\begin{aligned}\Delta(\Lambda, z_0) \approx & 0.1826 \pm 0.4315\mathrm{i}, -0.6956, -0.1160 \pm 1.0544\mathrm{i}, 1.0043, \\ & 1.0043, -0.1160 \pm 1.0544\mathrm{i}, -0.6956, 0.1826 \pm 0.4315\mathrm{i}\end{aligned}$$

when $t < 0$. Since these Δ values are different for different roots, outer lumps would experience different amounts of $O(1)$ position shifts according to formula (38).

The zero root of multiplicity six in $W_\Lambda(z)$ gives rise to an inner region of six fundamental lumps, whose positions are predicted by the roots of $Q_3(z)$ from Eq. (40). Here, we find from formula (109) that

$$\hat{\Delta} = 8/7, \tag{49}$$

which is independent of the root z_0 of $Q_3(z)$. Since this $\hat{\Delta}$ value is the same for all six roots of $Q_3(z)$, the six lumps in the inner region would experience the same amount of $O(1)$ position shift from formula (40).

Using the nonzero roots of $W_\Lambda(z)$ and roots of $Q_3(z)$, together with the above Δ and $\hat{\Delta}$ values, we can predict fundamental-lump locations from formulae (38) and (40) of Theorem 3, for the outer and inner regions, respectively. From that, we can draw the predicted solution in the (x, y) plane at any large time. When $t = \pm 10$, these predicted solutions are plotted in the left and right panels of Fig. 9, respectively. The predicted patterns contain twelve fundamental lumps which form a quasi-rectangular pattern in the outer region of the (x, y) plane, plus six fundamental lumps which form a triangle in the inner region. At $t = -10$, the outer lump pattern is roughly a stretching of $W_\Lambda(z)$'s nonzero-root structure, while the inner lump pattern is a stretching of $Q_3(z)$'s root structure. At $t = 10$, however, the predicted outer lump pattern has swapped its (x, y) axes from the $t = -10$ state [plus additional (x, y)-direction stretching], while the predicted inner triangular lump pattern has reversed its direction along the x-axis.

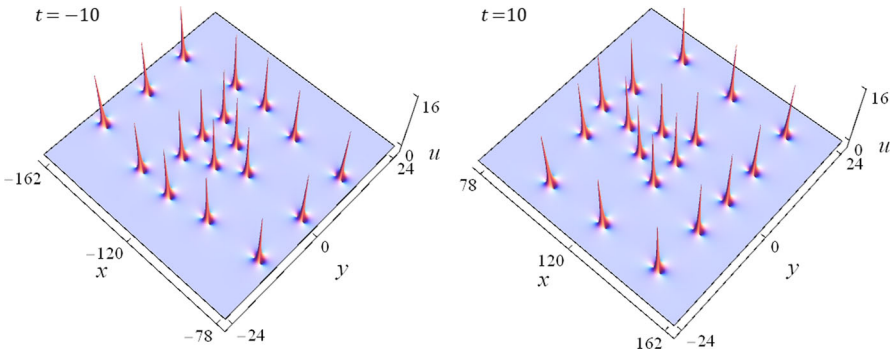

Fig. 9 Predicted solutions $u_\Lambda(x, y, t)$ with $\Lambda = (3, 4, 5, 7, 9)$ at time values of $t = -10$ (left) and $t = 10$ (right)

To confirm these asymptotic predictions, we plot in Fig. 10 the corresponding true solutions $u_\Lambda(x, y, t)$ at six time values of $t = -10, -2, -0.2, 0, 2$ and 10. In these true solutions, we have selected all-zero internal parameters of $\boldsymbol{a} = (0, 0, 0, 0, 0, 0, 0, 0, 0, 0)$. It is seen that at large times of $t = \pm 10$, the true solutions closely resemble our predictions in the previous figure. Specifically, the true solutions at these large times also split into outer and inner regions, with outer patterns quasi-rectangular and inner patterns triangular; and as time changes from $t = -10$ to $t = 10$, the outer pattern swaps its (x, y) orientations, while the inner pattern reverses in x-direction. All these features of the true solution match exactly our predictions in Fig. 9.

Next, we verify the error decay rate given in Eq. (42) of Theorem 3 for predictions in the inner region. At two time values of $t = 5$ and 15, both true solutions and predicted lump locations are shown on top of each other in the left and middle panels of Fig. 11, respectively. By visually comparing these two panels, we see that predicted lump positions at $t = 15$ are more accurate than at $t = 5$, meaning that the error decreases with time. To determine the error decay rate in the inner region, we plot in the right panel of Fig. 11 the error of prediction versus time for the inner lump marked by a white arrow in the mid-panel. This inner lump corresponds to a nonzero z_0 root of $Q_3(z)$. Thus, our analytical error decay rate for it from Eq. (42) is $O(|t|^{-1/3})$. The actual error graph in the right panel shows that its decay rate is indeed $O(|t|^{-1/3})$, confirming our theory. Thus, Theorem 3 for inner lumps associated with nonzero roots of $Q_{\hat{d}}(z)$ is numerically verified for $\Lambda = (3, 4, 5, 7, 9)$.

True solution graphs at intermediate time values in Fig. 10 reveal how these striking pattern transformations in outer and inner regions take place. It is seen that all fundamental lumps in the inner and outer regions at large negative time first move toward each other. Then, they merge and coalesce at $t \approx 0$. Afterward, all these fundamental lumps re-emerge and move away from each other, but not returning to their pre-merging state. Instead, the quasi-rectangular outer lumps have swapped their x and y directions, and the triangular inner lumps have reversed the x-direction. These pattern transformations are visually miraculous and mysterious. But due to our Theorem 3, they can now be completely understood from a mathematical point of view.

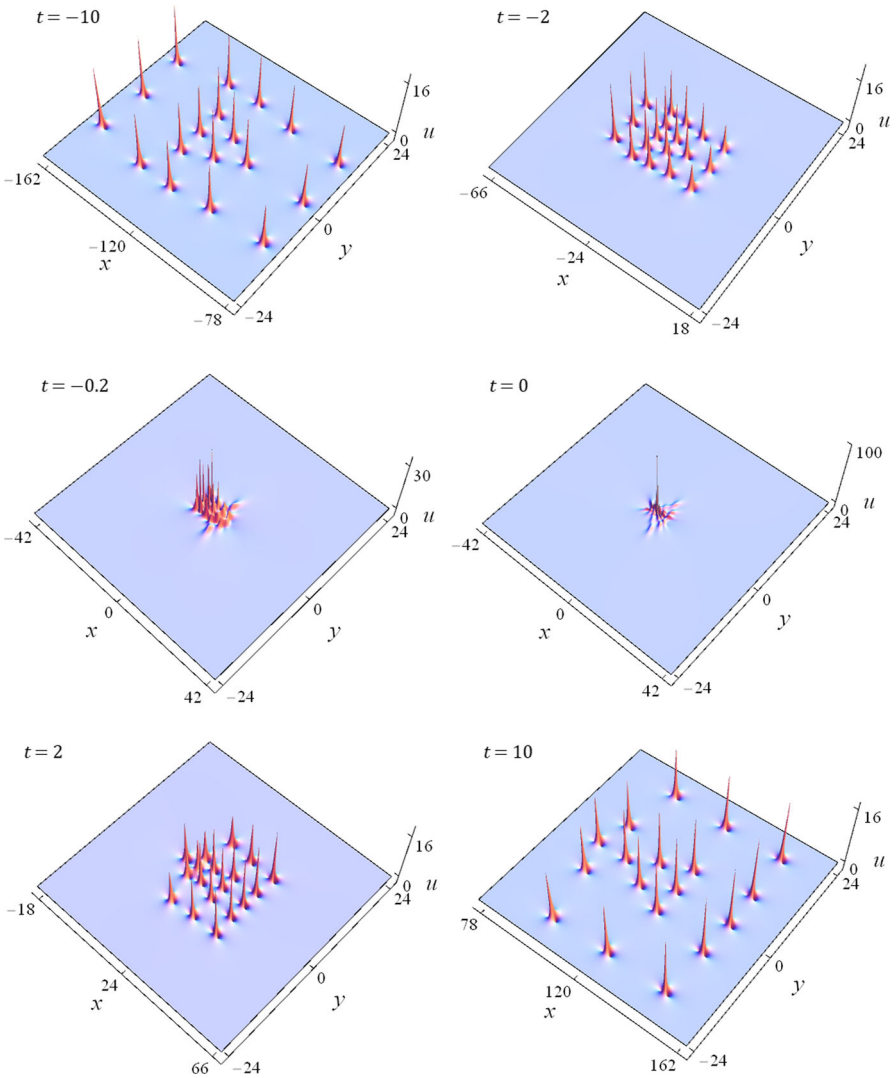

Fig. 10 True solutions $u_\Lambda(x, y, t)$ with $\Lambda = (3, 4, 5, 7, 9)$ and $\boldsymbol{a} = (0, 0, 0, 0, 0, 0, 0, 0, 0, 0)$, at various times whose values are shown inside the panels

Lastly, we have also numerically verified the $O(t^{-1})$ error decay rate of our prediction (42) in Theorem 3 for the inner lump associated with a zero root of $Q_{\hat{d}}(z)$ in Eq. (40), using $\Lambda = (1, 2, 3)$ as the example. Thus, the numerical verification of Theorem 3 is complete.

5 Proofs of the Two Theorems

Now, we prove our two theorems stated in Sect. 3. The reader is reminded that in these proofs, $p = 1$ and $\boldsymbol{a}_i$ are chosen as (33) in the higher-order lump solutions of

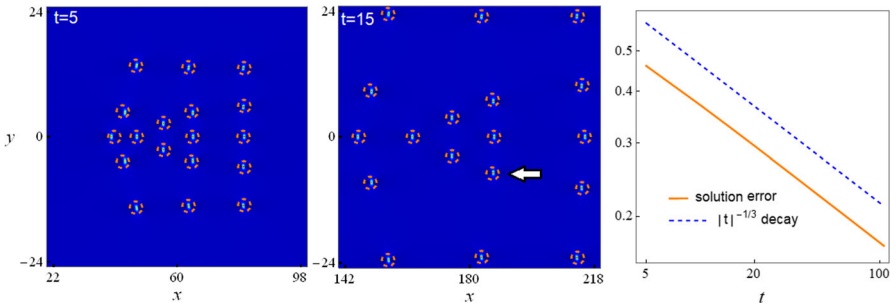

Fig. 11 Verification of the inner-region's error decay rate in Eq. (42) of Theorem 3 for the example of Fig. 10. The left and middle panels show density plots of true solutions, together with predicted locations of fundamental lumps marked by dashed circles, at $t = 5$ and 15, respectively. The right panel shows the decay rate of error versus t for the inner lump marked by a while arrow in mid-panel (the $|t|^{-1/3}$ decay is also plotted for comparison)

Theorem 1, for reasons which have been explained earlier in the paper. Thus, solution expressions in Theorem 1 can be simplified. Notably, the constant factor in Eq. (9) simplifies to $1/4^{\nu}$, and the $\boldsymbol{s}$ vector is real with $s_{\text{odd}} = 0$ (see the beginning of Sec. 3).

5.1 Proof of Theorem 2

In this case, $\Lambda = (1, 3, 5, \ldots, 2N-1)$. First, we rewrite the determinant (8) as a larger $3N \times 3N$ determinant (Ohta and Yang 2012; Yang and Yang 2021a)

$$\sigma = \begin{vmatrix} \mathbf{O}_{N\times N} & \Phi_{N\times 2N} \\ -\Psi_{2N\times N} & \mathbf{I}_{2N\times 2N} \end{vmatrix}, \tag{50}$$

where

$$\begin{aligned} \Phi_{i,j} &= 2^{-(j-1)} S_{2i-j} \left(\boldsymbol{x}^{+} + (j-1)\boldsymbol{s} + \boldsymbol{a}\right), \\ \Psi_{i,j} &= 2^{-(i-1)} S_{2j-i} \left((\boldsymbol{x}^{+})^{*} + (i-1)\boldsymbol{s} + \boldsymbol{a}^{*}\right), \end{aligned} \tag{51}$$

$S_j \equiv 0$ for $j < 0$, and vectors $\boldsymbol{x}^{+}$ and $\boldsymbol{s}$ are given in Eqs. (10) and (31). This determinant can be further simplified. Indeed, using the technique outlined in Appendix A of Yang and Yang (2021a), we can eliminate all x^{+}_{even} and a_{even} terms from the vectors $\boldsymbol{x}^{+}$ and $\boldsymbol{a}$, and reduce the above matrix element formulae to

$$\begin{aligned} \Phi_{i,j} &= 2^{-(j-1)} S_{2i-j} \left(\hat{\boldsymbol{x}}^{+} + (j-1)\boldsymbol{s} + \hat{\boldsymbol{a}}\right), \\ \Psi_{i,j} &= 2^{-(i-1)} S_{2j-i} \left((\hat{\boldsymbol{x}}^{+})^{*} + (i-1)\boldsymbol{s} + \hat{\boldsymbol{a}}^{*}\right), \end{aligned} \tag{52}$$

where

$$\hat{\boldsymbol{x}}^{+} \equiv \left(x_1^{+}, 0, x_3^{+}, 0, x_5^{+}, 0, \ldots\right), \quad \hat{\boldsymbol{a}} \equiv (0, 0, a_3, 0, a_5, 0, \ldots). \tag{53}$$

The elimination of the solution's dependence on x_2^+ is a key feature of the index vector $\Lambda = (1, 3, 5, \ldots, 2N-1)$, and this feature is responsible for the distinctive pattern behaviors described in Theorem 2.

Now, we analyze the large-time asymptotics of the above determinant σ. For this purpose, we introduce a moving x-frame coordinate

$$\hat{x} \equiv x - 12t. \tag{54}$$

Then, the elements x_k^+ in Eq. (10) become

$$x_1^+ = \hat{x} + 2\mathrm{i}y, \quad x_k^+ = \frac{1}{k!}\hat{x} + \frac{2^k}{k!}\mathrm{i}y + T_k, \tag{55}$$

where

$$T_k \equiv \frac{12(1-3^{k-1})}{k!}t. \tag{56}$$

In particular,

$$T_2 = -12t, \quad T_3 = -16t. \tag{57}$$

In this moving x-frame, when $|t|$ is large and $\sqrt{\hat{x}^2+y^2} = O(|t|^{1/3})$, we have the leading-order asymptotics for $S_k\left(\hat{\boldsymbol{x}}^+ + \nu\boldsymbol{s} + \hat{\boldsymbol{a}}\right)$ as

$$S_k\left(\hat{\boldsymbol{x}}^+ + \nu\boldsymbol{s} + \hat{\boldsymbol{a}}\right) \sim S_k(\mathbf{v}), \qquad |t| \gg 1, \tag{58}$$

where

$$\mathbf{v} = \left(x_1^+, 0, T_3, 0, 0, 0, \ldots\right). \tag{59}$$

By comparing the definition of Schur polynomials $S_k(\mathbf{v})$ to the definition of $p_k(z)$ polynomials in Eq. (17), we see that

$$S_k(\mathbf{v}) = (-3T_3/4)^{k/3} p_k(z), \tag{60}$$

where

$$z = (-3T_3/4)^{-1/3} x_1^+ = (-3T_3/4)^{-1/3}\left(\hat{x} + 2\mathrm{i}y\right). \tag{61}$$

Using these formulae and the Laplace expansion of the $3N \times 3N$ determinant (50)

$$\begin{aligned}\sigma = &\sum_{0\le\nu_1<\nu_2<\cdots<\nu_N\le 2N-1} \det_{1\le i,j\le N}\left(\frac{1}{2^{\nu_j}} S_{2i-1-\nu_j}(\hat{\boldsymbol{x}}^+ + \nu_j\boldsymbol{s} + \hat{\boldsymbol{a}})\right)\\ &\times \det_{1\le i,j\le N}\left(\frac{1}{2^{\nu_j}} S_{2i-1-\nu_j}[(\hat{\boldsymbol{x}}^+)^* + \nu_j\boldsymbol{s} + \hat{\boldsymbol{a}}^*]\right),\end{aligned} \tag{62}$$

together with the fact that the highest-order term of $|t|$ in this σ comes from the index choices of $\nu_j = j - 1$, we can readily show that the highest t-power term of σ is

$$\sigma \sim |\alpha_0|^2 \, |3T_3/4|^{\frac{N(N+1)}{3}} \, |Q_N(z)|^2 \,, \qquad |t| \gg 1, \tag{63}$$

where $\alpha_0 = 2^{-N(N-1)/2} c_N^{-1}$. Inserting this leading-order term of σ into Eq. (7), we see that the solution $u_\Lambda(x, y, t)$ approaches zero when $|t| \to \infty$, except at or near $(\hat{x}, y)$ locations (x_0, y_0), i.e., at or near (x, y) locations $(12t + x_0, y_0)$, where

$$z_0 = (-3T_3/4)^{-1/3} \, (x_0 + 2\mathrm{i} y_0) \tag{64}$$

is a root of the polynomial $Q_N(z)$. Solving this equation, we get the (x_0, y_0) locations given by Eq. (34) in Theorem 2. Due to our requirement of $\sqrt{\hat{x}^2 + y^2} = O(|t|^{1/3})$, z_0 in the above equation should be nonzero.

In order to derive the solution behavior near this $(x, y) = (12t + x_0, y_0)$ location, we need to perform a more refined asymptotic analysis and calculate the next-order terms in t, since the leading-order term in Eq. (63) vanishes at this point. Recalling $s_1 = 0$, this refined analysis is very similar to that we did for rogue waves in the NLS equation (Yang and Yang 2021a). For $z_0 \neq 0$ in the (x_0, y_0) formula (34), i.e., if the $(12t + x_0, y_0)$ location is $O(|t|^{1/3})$ away from the wave center $(12t, 0)$, then in the $O(1)$ neighborhood of $(12t + x_0, y_0)$, i.e., when $(x - 12t - x_0)^2 + (y - y_0)^2 = O(1)$, we have an asymptotics more refined than (58), which is

$$S_k\left(\hat{\boldsymbol{x}}^+ + \nu \boldsymbol{s} + \hat{\boldsymbol{a}}\right) = S_k(\mathbf{v}) \left(1 + O(|t|^{-2/3})\right). \tag{65}$$

This $O(|t|^{-2/3})$ relative error is due to our omission of $\hat{x}/6 + 4\mathrm{i}y/3$ relative to T_3 in x_3^+, and omission of x_5^+ relative to x_3^+. Using this refined asymptotics and repeating the same steps as in Yang and Yang (2021a), we find that

$$\sigma(x, y, t) = |\alpha_0|^2 \, \left|Q_N'(z_0)\right|^2 |3T_3/4|^{\frac{N(N+1)-2}{3}} \left((x - 12t - x_0)^2 + 4(y - y_0)^2 + \frac{1}{4}\right) \left(1 + O\left(|t|^{-1/3}\right)\right), \tag{66}$$

where α_0 is given below Eq. (63). For Yablonskii–Vorob'ev polynomials $Q_N(z)$, all roots are simple. Thus, $Q_N'(z_0) \neq 0$. Substituting this σ asymptotics into the solution expression (7) and performing a little simplification, we then get the asymptotics (35) for the $z_0 \neq 0$ case.

In the $O(1)$ neighborhood of the wave center $(12t, 0)$, where $(x - 12t)^2 + y^2 = O(1)$, we need to perform a separate asymptotic analysis, because the earlier S_k asymptotics (58) and (65) do not hold in this region. In this case, due to Eq. (55), when we lump T_{2k+1} and a_{2k+1} together in Eq. (52) and recall T_{2k+1} is proportional to t, the large-time analysis of the present σ determinant (50) is very similar to that in Appendix C of Yang and Yang (2021a) for the analysis of NLS rogue patterns when its internal parameters $(a_3, a_5, \ldots)$ are all large and of the same order. Repeating that analysis,

we find that if zero is not a root of $Q_N(z)$, then $\sigma(x, y, t) \sim \beta_0 |t|^{\frac{(N+2)(N-1)}{3}}$. But if zero is a root of $Q_N(z)$, i.e., $N \equiv 1 \bmod 3$, then

$$\sigma(x, y, t) = \beta_0 |t|^{\frac{N(N+1)-2}{3}} \left((x - 12t)^2 + 4y^2 + \frac{1}{4}\right)\left(1 + O\left(t^{-1}\right)\right), \quad (67)$$

where β_0 is a certain N-dependent positive constant. Substituting this σ asymptotics into the solution expression (7), we see that the leading-order term is the fundamental lump $u_1(x, y, t)$. Regarding the error of this leading-order approximation, Eq. (67) seems to suggest that the error would be $O(t^{-1})$. However, if the coefficient of the t^{-1} term in the last part of Eq. (67) is independent of x, then this t^{-1} term and 1 can be factored out and disappear after the variable transformation (7). In that case, the remaining terms from the last part of (67) would reduce to $1 + O(t^{-2})$, rendering the error of the leading-order approximation to be $O(t^{-2})$, or even smaller if the coefficient of the t^{-2} term in the last part of (67) is also independent of x. Thus, the error of this leading-order approximation for the center lump is $O(t^{-k})$ in general, where k is a certain positive integer. This proves the error estimate in Eq. (35) for the $z_0 = 0$ case. It is noted that we have specifically checked the solutions $u_\Lambda(x, y, t)$ for $N = 4$ and 7, and found that in both cases, errors of the leading-order approximation are $O(t^{-2})$. We suspect that this $O(t^{-2})$ error holds for the center lump at higher N values such as 10, 13, ... as well.

Theorem 2 is then proved.

5.2 Proof of Theorem 3

In this case, $\Lambda \neq (1, 3, 5, \ldots, 2N - 1)$. We first rewrite the determinant σ in (8) as a larger $(N + n_N + 1) \times (N + n_N + 1)$ determinant

$$\sigma = \begin{vmatrix} \mathbf{O}_{N\times N} & \Phi_{N\times(n_N+1)} \\ -\Psi_{(n_N+1)\times N} & \mathbf{I}_{(n_N+1)\times(n_N+1)} \end{vmatrix}, \quad (68)$$

where

$$\begin{aligned} \Phi_{i,j} &= 2^{-(j-1)} S_{n_i+1-j}\left(\boldsymbol{x}^+ + (j-1)\boldsymbol{s} + \boldsymbol{a}\right), \\ \Psi_{i,j} &= 2^{-(i-1)} S_{n_j+1-i}\left((\boldsymbol{x}^+)^* + (i-1)\boldsymbol{s} + \boldsymbol{a}^*\right), \end{aligned} \quad (69)$$

and vectors $\boldsymbol{x}^+$ and $\boldsymbol{s}$ are given in Eqs. (10) and (31). Unlike the previous case, we cannot eliminate x_2^+ from this solution now. Our large-time asymptotics of this determinant proceeds as follows.

5.2.1 Proof for the Outer Region

First, we prove the asymptotics (38)–(39) for the outer region. In this region, $\sqrt{\hat{x}^2 + y^2} = O(|t|^{1/2})$. Thus, we have the leading-order asymptotics for $S_k(\boldsymbol{x}^+ +$

$\nu \boldsymbol{s} + \boldsymbol{a}\big)$ as

$$S_k\left(\boldsymbol{x}^+ + \nu \boldsymbol{s} + \boldsymbol{a}\right) \sim S_k(\mathbf{w}), \qquad |t| \gg 1, \tag{70}$$

where

$$\mathbf{w} = \left(x_1^+,\, T_2,\, 0,\, 0,\, 0, \ldots\right), \tag{71}$$

and T_2 is as given in Eq. (57). By comparing the definition of Schur polynomials $S_k(\mathbf{w})$ to the definition of $q_k(z)$ polynomials in Eq. (20), we see that

$$S_k(\mathbf{w}) = T_2^{k/2} q_k(z), \tag{72}$$

where

$$z = T_2^{-1/2} x_1^+ = T_2^{-1/2}\left(\hat{x} + 2\mathrm{i}y\right). \tag{73}$$

Using these formulae and the Laplace expansion of the determinant (68) for σ, we can readily show that the highest t-power term of σ is

$$\sigma \sim |\mu_0|^2 \, |T_2|^{\rho} \, |W_\Lambda(z)|^2, \qquad |t| \gg 1, \tag{74}$$

where ρ is given in Eq. (13), and $\mu_0 = 2^{-N(N-1)/2}$. Inserting this leading-order term of σ into Eq. (7), we see that the solution $u_\Lambda(x, y, t)$ approaches zero when $|t| \to \infty$, except at or near $(\hat{x}, y)$ locations $\left(\hat{x}_0, \hat{y}_0\right)$, i.e., at or near (x, y) locations $\left(12t + \hat{x}_0, \hat{y}_0\right)$, where

$$z_0 = T_2^{-1/2}\left(\hat{x}_0 + 2\mathrm{i}\hat{y}_0\right) \tag{75}$$

is a root of the Wronskian–Hermit polynomial $W_\Lambda(z)$. Solving this equation, we get

$$\hat{x}_0 = \Re\left(z_0 T_2^{1/2}\right), \quad \hat{y}_0 = \frac{\Im\left(z_0 T_2^{1/2}\right)}{2}, \tag{76}$$

which are the leading-order terms of (x_0, y_0) in Eq. (38) of Theorem 3. Due to our requirement of $\sqrt{\hat{x}^2 + y^2} = O(|t|^{1/2})$, z_0 in the above equation should be nonzero.

To derive the solution behavior near this $(x, y) = \left(12t + \hat{x}_0, \hat{y}_0\right)$ location, we perform a more refined asymptotic analysis. Our starting point is a more accurate asymptotics for $S_k\left(\boldsymbol{x}^+ + \nu \boldsymbol{s} + \boldsymbol{a}\right)$,

$$S_k(\boldsymbol{x}^+ + \nu \boldsymbol{s} + \boldsymbol{a}) = S_k(\hat{\mathbf{w}})\left(1 + O\left(t^{-1}\right)\right), \qquad |t| \gg 1, \tag{77}$$

where

$$\hat{\mathbf{w}} = \left(x_1^+,\, x_2^+,\, T_3,\, 0,\, 0,\, 0, \ldots\right) = \mathbf{w} + \left(0, \hat{x}_2^+,\, T_3,\, 0,\, 0,\, 0, \ldots\right), \tag{78}$$

$\mathbf{w}$ is given in (71), and

$$\hat{x}_2^+ \equiv \frac{1}{2}\hat{x} + 2\mathrm{i}y. \tag{79}$$

The asymptotics (77) holds since $a_1 = s_1 = 0$. From the definition (6) of Schur polynomials and the above equation, we can relate $S_k(\hat{\mathbf{w}})$ and $S_k(\mathbf{w})$ as

$$S_k(\hat{\mathbf{w}}) = \sum_{j=0}^{k} b_j S_{k-j}(\mathbf{w}), \tag{80}$$

where b_j are the coefficients in the expansion

$$e^{\hat{x}_2^+\epsilon^2 + T_3\epsilon^3} = \sum_{j=0}^{\infty} b_j \epsilon^j. \tag{81}$$

Notice that $b_0 = 1$, $b_1 = 0$, $b_2 = \hat{x}_2^+$, and $b_3 = T_3$. In addition, $(\hat{x}, y) = O(|t|^{1/2})$ from Eq. (76), and $S_k(\mathbf{w}) = O(|t|^{k/2})$ in view of Eq. (72). Utilizing these relations, we find that

$$S_k(\boldsymbol{x}^+ + v\boldsymbol{s} + \boldsymbol{a}) = \left(S_k(\mathbf{w}) + \hat{x}_2^+ S_{k-2}(\mathbf{w}) + T_3 S_{k-3}(\mathbf{w})\right)\left(1 + O\left(t^{-1}\right)\right), \quad |t| \gg 1. \tag{82}$$

With this formula (82), we can now determine the asymptotic expression of σ in Eq. (68) in the neighborhood of $(x, y) = \left(12t + \hat{x}_0, \hat{y}_0\right)$ at large t. The Laplace expansion of this determinant is very similar to Eq. (62) of the previous subsection. Using this Laplace expansion and similar techniques as in Yang and Yang (2021a, 2021b), we can readily find that

$$\begin{aligned}\sigma(x, y, t) = |\mu_0|^2 \left|W_\Lambda'(z_0)\right|^2 |T_2|^{\rho-1} &\left(\left|(x - 12t - \hat{x}_0) + 2\mathrm{i}(y - \hat{y}_0) + \Delta\right|^2 + \frac{1}{4}\right) \\ &\times \left(1 + O\left(|t|^{-1/2}\right)\right),\end{aligned} \tag{83}$$

where μ_0 is given in Eq. (74), and $\Delta = \Delta(\Lambda, z_0)$ is a complex constant given by

$$\begin{aligned}\Delta = \frac{1}{W_\Lambda'(z_0)} &\left\{\lambda \sum_{j=1}^{N} \det_{1\le i\le N}\left(q_{n_i}, \ldots, q_{n_i-(j-2)}, q_{n_i-(j-1)-2}, q_{n_i-j}, \ldots, q_{n_i-(N-1)}\right)_{z=z_0}\right. \\ &\left. + \frac{4}{3}\sum_{j=1}^{N} \det_{1\le i\le N}\left(q_{n_i}, \ldots, q_{n_i-(j-2)}, q_{n_i-(j-1)-3}, q_{n_i-j}, \ldots, q_{n_i-(N-1)}\right)_{z=z_0}\right\},\end{aligned} \tag{84}$$

and

$$\lambda = \begin{cases} \frac{1}{2}\Re(z_0) + \mathrm{i}\Im(z_0), & \text{when } t < 0, \\ \Re(z_0) + \frac{1}{2}\mathrm{i}\Im(z_0), & \text{when } t > 0. \end{cases} \tag{85}$$

The former determinant in Eq. (84) is the Wronskian–Hermit determinant in Eq. (22) but with the j-th column $\{q_{n_i-(j-1)}\}$ replaced by $\{q_{n_i-(j-1)-2}\}$, i.e., reducing the subscript value of this column by two, while the latter determinant in (84) is the Wronskian–Hermit determinant (22) with the j-th column replaced by $\{q_{n_i-(j-1)-3}\}$, i.e., reducing its subscript value by three.

The complex constant Δ in Eq. (83) can be absorbed into $(\hat{x}_0, \hat{y}_0)$. After this absorption and rearranging terms, Eq. (83) becomes

$$\sigma(x, y, t) = |\mu_0|^2 \left|W'_\Lambda(z_0)\right|^2 |T_2|^{\rho-1} \times \left((x - 12t - x_0)^2 + 4(y - y_0)^2 + \frac{1}{4}\right)\left(1 + O\left(|t|^{-1/2}\right)\right), \tag{86}$$

where (x_0, y_0) are as given in Eq. (38) of Theorem 3. Substituting this σ asymptotics into Eq. (7), the asymptotics (38)–(39) for the outer region of Theorem 3 are then proved.

5.2.2 Proof for the Inner Region

In the inner region, where $\sqrt{\hat{x}^2 + y^2} \le O(|t|^{1/3})$, a separate asymptotic analysis is needed, because the previous S_k asymptotics (70) and (77) do not hold.

When $\sqrt{\hat{x}^2 + y^2} = O(|t|^{1/3})$, since $a_1 = s_1 = 0$, we see that

$$S_k(\boldsymbol{x}^+ + v\boldsymbol{s} + \boldsymbol{a}) = S_k(\mathbf{h})\left(1 + O\left(|t|^{-2/3}\right)\right), \tag{87}$$

where

$$\mathbf{h} = (x_1^+, T_2, T_3, 0, 0, \ldots). \tag{88}$$

Splitting $\mathbf{h}$ as

$$\mathbf{h} = (0, T_2, 0, 0, \ldots) + \hat{\mathbf{h}}, \tag{89}$$

with $\hat{\mathbf{h}} \equiv (x_1^+, 0, T_3, 0, 0, \ldots)$, we can use definition (6) of Schur polynomials to show that

$$S_k(\mathbf{h}) = \sum_{j=0}^{[k/2]} \frac{T_2^j}{j!} S_{k-2j}(\hat{\mathbf{h}}), \tag{90}$$

where $[a]$ represents the largest integer less than or equal to a. In addition, by comparing the definition of $S_k(\hat{\mathbf{h}})$ with $p_k(z)$ in Eq. (17) and through variable scalings, we see that

$$S_k(\hat{\mathbf{h}}) = (-3T_3/4)^{k/3}\, p_k(z), \tag{91}$$

where z is as given in Eq. (61).

Now, we use the above asymptotics to derive the highest-power term of t in σ of Eq. (68). For this purpose, we reorganize the rows of Φ by grouping odd-n_i rows together (in ascending order of n_i), followed by even-n_i rows (also in ascending order of n_i). Similar groupings would also be applied to the columns of Ψ in (68). These simultaneous row and column exchanges do not affect the σ determinant. After such regrouping, we can assume that $n_1 < n_2 < \cdots < n_l$ are all odd indices, and $n_{l+1} < n_{l+2} < \cdots < n_N$ are all even indices, where $l = k_{\text{odd}}$. We also rewrite $S_k(\boldsymbol{x}^+ + \nu \boldsymbol{s} + \boldsymbol{a})$ in terms of $S_k(\hat{\mathbf{h}})$ through Eqs. (87) and (90) as

$$\Phi = \begin{pmatrix} D_1 A_1 E_1 \Phi_1 \\ D_2 A_2 E_2 \Phi_2 \end{pmatrix} \left(1 + O\left(|t|^{-2/3}\right)\right), \tag{92}$$

where

$$\begin{aligned} D_1 &= \operatorname{diag}\left(T_2^{\frac{1}{2}(n_1-1)}, T_2^{\frac{1}{2}(n_2-1)}, \cdots T_2^{\frac{1}{2}(n_l-1)}\right), \\ E_1 &= \operatorname{diag}\left(1, T_2^{-1}, T_2^{-2}, \ldots, T_2^{-\frac{1}{2}(n_l-1)}\right), \end{aligned} \tag{93}$$

$$\begin{aligned} D_2 &= \operatorname{diag}\left(T_2^{\frac{1}{2}n_{l+1}}, T_2^{\frac{1}{2}n_{l+2}}, \ldots T_2^{\frac{1}{2}n_N}\right), \\ E_2 &= \operatorname{diag}\left(1, T_2^{-1}, T_2^{-2}, \ldots, T_2^{-\frac{1}{2}n_N}\right), \end{aligned} \tag{94}$$

$$A_1 = \begin{pmatrix} \frac{1}{\left(\frac{1}{2}(n_1-1)\right)!} & \frac{1}{\left(\frac{1}{2}(n_1-1)-1\right)!} & \frac{1}{\left(\frac{1}{2}(n_1-1)-2\right)!} & \cdots \\ \frac{1}{\left(\frac{1}{2}(n_2-1)\right)!} & \frac{1}{\left(\frac{1}{2}(n_2-1)-1\right)!} & \frac{1}{\left(\frac{1}{2}(n_2-1)-2\right)!} & \cdots \\ \vdots & \vdots & \vdots & \vdots \\ \frac{1}{\left(\frac{1}{2}(n_l-1)\right)!} & \frac{1}{\left(\frac{1}{2}(n_l-1)-1\right)!} & \frac{1}{\left(\frac{1}{2}(n_l-1)-2\right)!} & \cdots \end{pmatrix}_{l \times \frac{1}{2}(n_l+1)}, \tag{95}$$

$$A_2 = \begin{pmatrix} \frac{1}{\left(\frac{1}{2}n_{l+1}\right)!} & \frac{1}{\left(\frac{1}{2}n_{l+1}-1\right)!} & \frac{1}{\left(\frac{1}{2}n_{l+1}-2\right)!} & \cdots \\ \frac{1}{\left(\frac{1}{2}n_{l+2}\right)!} & \frac{1}{\left(\frac{1}{2}n_{l+2}-1\right)!} & \frac{1}{\left(\frac{1}{2}n_{l+2}-2\right)!} & \cdots \\ \vdots & \vdots & \vdots & \vdots \\ \frac{1}{\left(\frac{1}{2}n_N\right)!} & \frac{1}{\left(\frac{1}{2}n_N-1\right)!} & \frac{1}{\left(\frac{1}{2}n_N-2\right)!} & \cdots \end{pmatrix}_{(N-l)\times\left(\frac{1}{2}n_N+1\right)}, \tag{96}$$

$$\begin{aligned} \Phi_1(i,j) &= 2^{-(j-1)} S_{2i-j}(\hat{\mathbf{h}}), \\ \Phi_2(i,j) &= 2^{-(j-1)} S_{2i-j-1}(\hat{\mathbf{h}}). \end{aligned} \tag{97}$$

In matrices A_1 and A_2 here, we have defined $1/0! \equiv 1$ and $1/k! \equiv 0$ if $k < 0$. We further perform LU decomposition for matrices A_1 and A_2,

$$A_1 = L_1 U_1, \quad A_2 = L_2 U_2, \tag{98}$$

where L_1, L_2 are square lower-triangular matrices, and U_1, U_2 are matrices of the same dimensions as A_1, A_2 with $U_k(i, j) = 0$ if $j > i$. By normalization, we make $U_k(i, i) = 1$. Thus,

$$U_1 = \begin{pmatrix} 1 & \alpha_1 & \cdots & \cdots & \cdots \\ 0 & 1 & \alpha_2 & \cdots & \cdots \\ \vdots & \ddots & \ddots & \ddots & \ddots \\ 0 & \cdots & 0 & 1 & \alpha_{k_{\text{odd}}} \end{pmatrix}, \quad U_2 = \begin{pmatrix} 1 & \beta_1 & \cdots & \cdots & \cdots \\ 0 & 1 & \beta_2 & \cdots & \cdots \\ \vdots & \ddots & \ddots & \ddots & \ddots \\ 0 & \cdots & 0 & 1 & \beta_{k_{\text{even}}} \end{pmatrix}. \tag{99}$$

Now, we use these results to derive the highest-power term of t in σ of Eq. (68). It is easy to see from the Laplace expansion of the σ determinant (68) that, at large $|t|$, the highest t-power term of σ comes from the index choice of $\nu_j = j - 1$, i.e.,

$$\sigma \sim \left| \det_{1 \le i,j \le N} \left(\frac{1}{2^{j-1}} S_{n_i+1-j}(\boldsymbol{x}^+ + (j-1)\boldsymbol{s} + \boldsymbol{a}) \right) \right|^2, \qquad |t| \gg 1. \tag{100}$$

Inserting Eqs. (91)–(92) into this expression, we find that the highest t-power term of σ is

$$\sigma \sim \gamma_0 \, |T_2|^{N_W} |3T_3/4|^{\frac{\hat{d}(\hat{d}+1)}{3}} \, |H(z)|^2 , \tag{101}$$

where $\gamma_0 = \det(L_1)^2 \det(L_2)^2$ is a nonzero positive constant, N_W is given in Eq. (24), $\hat{d}$ is defined in Eq. (41), and $H(z)$ is the Wronskian determinant

$$H(z) = \det \begin{pmatrix} p_1(z) & p_0(z) & p_{-1}(z) & \cdots \\ p_3(z) & p_2(z) & p_1(z) & \cdots \\ \vdots & \vdots & \vdots & \vdots \\ p_{2k_{\text{odd}}-1}(z) & p_{2k_{\text{odd}}-2}(z) & p_{2k_{\text{odd}}-3}(z) & \cdots \\ p_0(z) & p_{-1}(z) & p_{-2}(z) & \cdots \\ p_2(z) & p_1(z) & p_0(z) & \cdots \\ \vdots & \vdots & \vdots & \vdots \\ p_{2k_{\text{even}}-2}(z) & p_{2k_{\text{even}}-3}(z) & p_{2k_{\text{even}}-4}(z) & \cdots \end{pmatrix}, \tag{102}$$

i.e.,

$$H(z) = \text{Wron}\left[p_1(z), p_3(z), \ldots, p_{2k_{\text{odd}}-1}(z), p_0(z), p_2(z), \ldots, p_{2k_{\text{even}}-2}(z) \right]. \tag{103}$$

This H determinant can be reduced to

$$H(z) = (-1)^{\hat{k}} Q_{\hat{d}}(z), \tag{104}$$

where $\hat{k}$ is a certain integer which counts the number of row permutations in order to reduce $H(z)$ to $Q_{\hat{d}}(z)$. Thus, when $\sqrt{\hat{x}^2+y^2}=O(|t|^{1/3})$,

$$\sigma \sim \gamma_0 |T_2|^{N_W} |3T_3/4|^{\frac{\hat{d}(\hat{d}+1)}{3}} \left|Q_{\hat{d}}(z)\right|^2. \tag{105}$$

In view of Eqs. (7) and (61), this asymptotics shows that the solution $u_\Lambda(x,y,t)$ is asymptotically zero in this region, except when $\hat{d}>0$ (i.e., zero is a root of $W_\Lambda(z)$), and when (x,y) is at or near the location $\left(12t+\hat{x}_0,\hat{y}_0\right)$, where

$$z_0=(-3T_3/4)^{-1/3}\left(\hat{x}_0+2\mathrm{i}\hat{y}_0\right) \tag{106}$$

is a root of $Q_{\hat{d}}(z)$. Solving this equation, we get $(\hat{x}_0,\hat{y}_0)$ values that are the leading-order terms in Eq. (40) of Theorem 3. Since $\sqrt{\hat{x}^2+y^2}=O(|t|^{1/3})$, root z_0 in the above equation should be nonzero.

We can further show that near this $(x,y)=\left(12t+\hat{x}_0,\hat{y}_0\right)$ location lies a fundamental lump. This calculation is similar to what we did in the proof of Theorem 2 and the earlier part of this proof for Theorem 3. Specifically, we can see from Eq. (92) that

$$\Phi=\begin{pmatrix} L_1 & \mathbf{0} \\ \mathbf{0} & L_2 \end{pmatrix} \begin{pmatrix} S_1(\hat{\mathbf{h}})+\alpha_1 T_2^{-1} S_3(\hat{\mathbf{h}}) & S_0(\hat{\mathbf{h}})+\alpha_1 T_2^{-1} S_2(\hat{\mathbf{h}}) & \cdots \\ S_3(\hat{\mathbf{h}})+\alpha_2 T_2^{-1} S_5(\hat{\mathbf{h}}) & S_2(\hat{\mathbf{h}})+\alpha_2 T_2^{-1} S_4(\hat{\mathbf{h}}) & \cdots \\ \vdots & \vdots & \vdots \\ S_{2k_{\text{odd}}-1}(\hat{\mathbf{h}})+\alpha_{k_{\text{odd}}} T_2^{-1} S_{2k_{\text{odd}}+1}(\hat{\mathbf{h}}) & S_{2k_{\text{odd}}-2}(\hat{\mathbf{h}})+\alpha_{k_{\text{odd}}} T_2^{-1} S_{2k_{\text{odd}}}(\hat{\mathbf{h}}) & \cdots \\ S_0(\hat{\mathbf{h}})+\beta_1 T_2^{-1} S_2(\hat{\mathbf{h}}) & \beta_1 T_2^{-1} S_1(\hat{\mathbf{h}}) & \cdots \\ S_2(\hat{\mathbf{h}})+\beta_2 T_2^{-1} S_4(\hat{\mathbf{h}}) & S_1(\hat{\mathbf{h}})+\beta_2 T_2^{-1} S_3(\hat{\mathbf{h}}) & \cdots \\ \vdots & \vdots & \vdots \\ S_{2k_{\text{even}}}(\hat{\mathbf{h}})+\beta_{k_{\text{even}}} T_2^{-1} S_{2k_{\text{even}}+2}(\hat{\mathbf{h}}) & S_{2k_{\text{even}}-1}(\hat{\mathbf{h}})+\beta_{k_{\text{even}}} T_2^{-1} S_{2k_{\text{even}}+1}(\hat{\mathbf{h}}) & \cdots \end{pmatrix} \left(1+O\left(|t|^{-2/3}\right)\right). \tag{107}$$

Using this result and the connection between $S_k(\hat{\mathbf{h}})$ and $p_k(z)$ in Eq. (91), we can show that in the $O(1)$ neighborhood of the above $(\hat{x}_0,\hat{y}_0)$ location,

$$\begin{aligned}\sigma(x,y,t)=\gamma_0|T_2|^{N_W}|3T_3/4|^{\frac{\hat{d}(\hat{d}+1)-2}{3}}\left|Q'_{\hat{d}}(z_0)\right|^2 \\ \times\left(\left|(x-12t-\hat{x}_0)+2\mathrm{i}(y-\hat{y}_0)+\hat{\Delta}\right|^2+\frac{1}{4}\right)\left(1+O\left(|t|^{-1/3}\right)\right),\end{aligned} \tag{108}$$

where

$$\hat{\Delta}=-\frac{\alpha_{k_{\text{odd}}}H_1(z_0)+\beta_{k_{\text{even}}}H_2(z_0)}{H'(z_0)}, \tag{109}$$

$H_1(z)$ is the H determinant in (102) with its k_{odd}-th row replaced by the row vector $(p_{2k_{\text{odd}}+1}(z),\ p_{2k_{\text{odd}}},\ p_{2k_{\text{odd}}-1}(z),\ldots)$, i.e., with the subscripts of the k_{odd}-th row of H increased by two, and $H_2(z)$ is the H determinant in (102) with its last row replaced by

the vector $(p_{2k_{\text{even}}}(z), p_{2k_{\text{even}}-1}, p_{2k_{\text{even}}-2}(z), \ldots)$, i.e., with the subscripts of its last row increased by two. In other words,

$$H_1(z) = \text{Wron}\left[p_1(z), p_3(z), \ldots, p_{2k_{\text{odd}}-3}(z), p_{2k_{\text{odd}}+1}(z), p_0(z), p_2(z), \ldots, p_{2k_{\text{even}}-2}(z)\right], \quad (110)$$

$$H_2(z) = \text{Wron}\left[p_1(z), p_3(z), \ldots, p_{2k_{\text{odd}}-1}(z), p_0(z), p_2(z), \ldots, p_{2k_{\text{even}}-4}(z), p_{2k_{\text{even}}}(z)\right]. \quad (111)$$

Note that the negative sign in (109) is induced by the negative sign in the relation (91). This $\hat{\Delta}$ is a constant, which is the analog of a similar quantity Δ we derived in Eq. (84) for a fundamental lump in the outer region.

It is easy to see that the above $\sigma(x, y, t)$ gives a fundamental lump, whose position is at $(x, y) = (12t + x_0, y_0)$, where (x_0, y_0) are as given in Eq. (40) of Theorem 3. In addition, the error of this prediction is $O\left(|t|^{-1/3}\right)$.

In the center region where $\hat{x}^2 + y^2 = O(1)$, we can use the technique of Appendix C in Yang and Yang (2021a) to show that at large time, if zero is a root of $Q_{\hat{d}}(z)$, i.e., if $\hat{d} \equiv 1 \bmod 3$, then $u_\Lambda(x, y, t)$ would approach a fundamental lump located in the $O(1)$ neighborhood of the wave center $(\hat{x}, y) = (0, 0)$, whose location is predicted in Eq. (40) by setting $z_0 = 0$ and $\hat{\Delta} = \hat{\Delta}|_{z_0=0}$, where $\hat{\Delta}(\Lambda, z_0)$ is given in Eq. (109). If zero is not a root of $Q_{\hat{d}}(z)$, then $u_\Lambda(x, y, t)$ would approach zero in this center region as $|t| \to \infty$. Details will be omitted for brevity. It may be more illuminating for us to point out that the leading-order term of the previous asymptotic formula (108), which was derived for the region of $\sqrt{\hat{x}^2 + y^2} = O(|t|^{1/3})$ and nonzero roots z_0 of $Q_{\hat{d}}(z)$, turns out to be valid for the $\hat{x}^2 + y^2 = O(1)$ region and the zero root z_0 of $Q_{\hat{d}}(z)$ as well [except for the error term, which is now $O(t^{-1})$ rather than $O(|t|^{-1/3})$]. In other words, if zero is a root of $Q_{\hat{d}}(z)$, then setting $z_0 = 0$ in the leading term of (108), we would get the correct asymptotic fundamental lump in the center region.

Lastly, we note that when (x, y) is between the outer and inner regions, i.e., when $\sqrt{\hat{x}^2 + y^2} = O\left(|t|^q\right)$ where $1/3 < q < 1/2$, or outside the outer region, i.e., when $\sqrt{\hat{x}^2 + y^2} > O\left(|t|^{1/2}\right)$, we can show through some algebra that the solution u_Λ would approach zero when $|t| \to \infty$. Thus, there are no additional lumps in the (x, y) plane except for the ones identified in Eqs. (38) and (40). This completes the proof of Theorem 3.

Before ending this section, we would like to make a remark concerning $\hat{\Delta}$. The formula (109) seems to show that $\hat{\Delta} = \hat{\Delta}(\Lambda, z_0)$, i.e., $\hat{\Delta}$ depends on both Λ and z_0. Its dependence on Λ is certain, not only because $H(z)$, $H_1(z)$ and $H_2(z)$ depend on Λ, but also because the coefficients $\alpha_{k_{\text{odd}}}$ and $\beta_{k_{\text{even}}}$ in (109) are determined by Λ as well through the LU factorization (98). For example, if $\Lambda = (3, 4, 5, 7, 9)$ as we have used before, then $\alpha_{k_{\text{odd}}} = \alpha_4 = 4$, and $\beta_{k_{\text{even}}} = \beta_1 = 2$. For other Λ vectors, $\alpha_{k_{\text{odd}}}$ and $\beta_{k_{\text{even}}}$ would generally be different. However, the dependence of $\hat{\Delta}(\Lambda, z_0)$ on z_0 is less certain despite its appearance. For $\Lambda = (3, 4, 5, 7, 9)$, we find that the $H(z)$, $H_1(z)$ and $H_2(z)$ polynomials are related as

$$H_1(z) = -H_2(z) = \lambda_0 \left(z^2 H(z) - 8H'(z)\right), \quad (112)$$

where $\lambda_0 = 1/14$. Since z_0 is a root of $H(z)$, using these relations we can quickly find from Eq. (109) that

$$\hat{\Delta} = 8\lambda_0 \left(\alpha_{k_{\text{odd}}} - \beta_{k_{\text{even}}}\right), \tag{113}$$

which gives $\hat{\Delta} = 8/7$ that is independent of z_0. We have checked a number of other index vectors Λ as well, and found that in all checked cases, the above relations (112) always hold, except that the constant coefficient λ_0 generally differs for other Λ vectors. Note that if k_{odd} or k_{even} is zero, then there will be no $H_1(z)$ and $\alpha_{k_{\text{odd}}}$, or $H_2(z)$ and $\beta_{k_{\text{even}}}$, in which case the rest of the relations in (112) still held in the examples we checked. We conjecture that these algebraic relations (112) between $H(z)$, $H_1(z)$ and $H_2(z)$ polynomials are valid for all Λ vectors. If so, then $\hat{\Delta}$ would be given by Eq. (113), which is always z_0-independent, i.e., $\hat{\Delta} = \hat{\Delta}(\Lambda)$. In this case, the $O(1)$ position shifts in formula (40) would be identical for all inner lumps, which implies that the inner lump pattern would be the triangular shape of the Yablonskii–Vorob'ev root structure without deformation.

5.3 Time of Asymptotic Validity for Theorems 2 and 3

Theorems 2 and 3 are derived under the condition that $|t|$ is large and $\boldsymbol{a}$ is a constant vector. If all a_k in $\boldsymbol{a}$ are $O(1)$ or smaller, these theorems will hold when $|t| \gg 1$. But if some of the a_k's are large, such as in the solution of Fig. 7, how large would $|t|$ need to be in order for these theorems to remain valid? We address this question below.

First, we consider Theorem 2. In its proof, the key asymptotic relation we used is Eq. (65), i.e.,

$$S_k\left(\hat{\boldsymbol{x}}^+ + v\boldsymbol{s} + \hat{\boldsymbol{a}}\right) = S_k\left(x_1^+, 0, T_3, 0, 0, 0, \ldots\right)\left(1 + O(|t|^{-2/3})\right), \tag{114}$$

from which the rest of the calculation follows. Notice that when $\sqrt{\hat{x}^2 + y^2} = O(|t|^{1/3})$,

$$S_k\left(\hat{\boldsymbol{x}}^+ + v\boldsymbol{s} + \hat{\boldsymbol{a}}\right) = S_k\left(x_1^+, 0, T_3 + a_3, 0, a_5, 0, \ldots\right)\left(1 + O\left(|t|^{-2/3}\right)\right). \tag{115}$$

In addition, from the definition (6) of Schur polynomials, we have

$$S_k\left(x_1^+, 0, T_3 + a_3, 0, a_5, 0, \ldots\right) = \epsilon^{-k} S_k\left(x_1^+\epsilon, 0, (T_3 + a_3)\epsilon^3, 0, a_5\epsilon^5, 0, \ldots\right), \tag{116}$$

where ϵ is an arbitrary constant. Choosing $\epsilon = T_3^{-1/3}$, then if

$$\left|a_{2k+1} T_3^{-(2k+1)/3}\right| \le O\left(T_3^{-2/3}\right), \quad k \ge 1, \tag{117}$$

or, equivalently,

$$|t| \geq O\left(\frac{1}{16}\,|a_{2k+1}|^{\frac{3}{2k-1}}\right), \quad k \geq 1, \tag{118}$$

the right side of (116) would reduce to

$$\begin{aligned} &T_3^{k/3} S_k\left(x_1^+ T_3^{-1/3}, 0, 1, 0, 0, 0, \ldots\right)\left(1 + O\left(|T_3|^{-2/3}\right)\right) \\ &\quad = S_k\left(x_1^+, 0, T_3, 0, 0, 0, \ldots\right)\left(1 + O\left(|T_3|^{-2/3}\right)\right). \end{aligned} \tag{119}$$

Thus, the asymptotic relation (114) still holds. This means that if parameters a_{2k+1} are large, then Theorem 2 would be valid when $|t|$ is suitably large according to Eq. (118). Notice that this time condition will be weaker if k is larger. For instance, if $k = 3$, i.e., $|a_7|$ is large, then Theorem 2 would be valid when $|t| \geq O\left(|a_7|^{3/5}/16\right)$.

Next, we consider Theorem 3. In the outer region, the key asymptotic relation we used is Eq. (77), while in the inner region, the key asymptotics used is Eq. (87). Using similar arguments as above, we can show that the outer asymptotics (77), and hence the outer-region prediction (39) in Theorem 3, would remain valid if

$$|a_k| \leq O\left(T_2^{(k-2)/2}\right), \quad k = 2, 3, \ldots, \tag{120}$$

or equivalently,

$$|a_2| \leq O(1), \quad |t| \geq O\left(\frac{1}{12}\,|a_k|^{\frac{2}{k-2}}\right), \quad k \geq 3. \tag{121}$$

For example, if $|a_5|$ is large and all other a_k's are $O(1)$ or smaller, as in Figs. 7 and 8, then the outer-region prediction (39) will hold when

$$|t| \geq O\left(\frac{1}{12}|a_5|^{2/3}\right). \tag{122}$$

If $|a_2|$ is large, then its negligence from $x_2^+ + \nu s_2 + a_2$, i,e., from $T_2 + \hat{x}_2^+ + \nu s_2 + a_2$, produces a relative error of a_2/T_2, since T_2 is the leading-order term here. This relative error of a_2/T_2 will propagate down later calculations and result in an absolute error of $O(a_2|t|^{-1/2})$ to the outer asymptotics (39). In other words, when $|a_2|$ is large, the error $O\left(|t|^{-1/2}\right)$ in the outer asymptotics (39) would be replaced by $O(a_2|t|^{-1/2})$. In this case, $|t|$ will need to be much larger than $|a_2|^2$ in order for the error to be small.

Regarding the inner asymptotics (87), and hence the inner-region prediction (42) in Theorem 3, they would remain valid if

$$|a_2| \leq O\left(T_3^{1/3}\right), \quad |a_k| \leq O\left(T_3^{(k-2)/3}\right), \quad k \geq 3, \tag{123}$$

or equivalently,

$$|t| \geq O\left(\frac{1}{16}\,|a_2|^3\right), \quad \text{and} \quad |t| \geq O\left(\frac{1}{16}\,|a_k|^{\frac{3}{k-2}}\right), \quad k \geq 3. \tag{124}$$

6 Summary and Discussion

In this article, we have analytically studied pattern formation in higher-order lumps of the KP-I equation at large time. For a broad class of these higher-order lumps, we have shown that two types of solution patterns appear at large time. The first type of patterns comprise fundamental lumps arranged in triangular shapes, which are described analytically by root structures of Yablonskii–Vorob'ev polynomials. As time evolves from large negative to large positive, this triangular pattern reverses its x-direction. The second type of solution patterns comprise fundamental lumps arranged in non-triangular shapes in the outer region, which are described analytically by nonzero-root structures of Wronskian–Hermit polynomials, together with possible fundamental lumps arranged in triangular shapes in the inner region, which are described analytically by root structures of Yablonskii–Vorob'ev polynomials. When time evolves from large negative to large positive, the non-triangular pattern in the outer region switches its x and y directions, while the triangular pattern in the inner region reverses its x-direction. We have also compared these predicted patterns with true solutions, and excellent agreement is observed.

In this pattern analysis of higher-order lumps, we have set the spectral parameter $p = 1$ without any loss of generality (see Remark 5 of Sect. 2). Because of this, lump patterns we have predicted at large time are all y-symmetric (see Figs. 3, 6 and 9), since root structures of Yablonskii–Vorob'ev and Wronskian–Hermit polynomials are symmetric with respect to the real-z axis. However, under the Galilean transformation (4), these y-symmetric lump patterns can become skewed and y-asymmetric, and these y-asymmetric patterns correspond to complex spectral parameters p. Thus, y-asymmetric lump patterns also exist in the KP-I equation, and such patterns can be obtained from the y-symmetric ones through the Galilean transformation.

Are there other patterns of higher-order lumps at large time? The answer is yes. Notice that in this article, we have assumed internal-parameter vectors $\boldsymbol{a}_i$ of higher-order lumps to be equal to each other [see Eq. (33)]. If these parameter vectors are allowed to differ from each other, then the analytical results at large time will become different. This problem will not be pursued in this paper, and will be left for future studies.

In a very recent preprint (Dong et al. 2021), the authors also derived higher-order lumps in the KP-I equation and studied their large-time patterns through Darboux transformation, and showed that their large-time patterns are described analytically by root structures of Yablonskii–Vorob'ev polynomials. Obviously, the higher-order lump solutions they derived are a very special class of solutions which correspond to the index vector $\Lambda = (1, 3, 5, \ldots, 2N-1)$ and under $\boldsymbol{a}_i$ parameter constraints (33) in our general solutions of Theorem 1, and their large-time pattern results are largely equivalent to our Theorem 2. However, their error estimate of $O(|t|^{-2/3})$ for

fundamental-lump predictions far away from the wave center is different from our $O(|t|^{-1/3})$ in Theorem 2, and we have verified numerically that our error estimate is correct, not theirs. (Our numerical verification result is shown in Fig. 5.) More importantly, those authors have not considered the more general higher-order lumps corresponding to the index vector $\Lambda \neq (1, 3, 5, \ldots, 2N-1)$ in our Theorem 1, nor their large-time solution patterns. These latter patterns are the contents of our Theorem 3 (see also our Figs. 6, 7, 8, 9, 10, 11).

Acknowledgements This material is based on work supported by the National Science Foundation under Award Number DMS-1910282, and the Air Force Office of Scientific Research under Award Number FA9550-18-1-0098.

Data Availability All data generated or analyzed during this study are included in this published article.

Appendix

In this appendix, we briefly derive the bilinear higher-order lump solutions presented in Theorem 1.

Under the variable transformation $u = 2(\log\tau)_{xx}$ and notations of $x_1 = x$, $x_2 = \mathrm{i}y$ and $x_3 = -4t$, the KP-I equation (3) is converted to the bilinear equation

$$(D_{x_1}^4 - 4D_{x_1}D_{x_3} + 3D_{x_2}^2)\,\tau\cdot\tau = 0, \tag{125}$$

where D is Hirota's bilinear differential operator. It is well-known that if m_{ij}, ϕ_i and ψ_j are functions of (x_1, x_2, x_3) and satisfy the following differential equations

$$\partial_{x_1} m_{ij} = \phi_i\psi_j, \tag{126}$$
$$\partial_{x_n}\phi_i = \partial_{x_1}^n\phi_i, \qquad n = 2, 3, \tag{127}$$
$$\partial_{x_n}\psi_j = (-1)^{n-1}\partial_{x_1}^n\psi_j, \quad n = 2, 3, \tag{128}$$

then the τ function

$$\tau = \det_{1\le i,j\le N}\left(m_{ij}\right) \tag{129}$$

would satisfy the above bilinear equation (Hirota 2004). To derive higher-order lump solutions, we define m_{ij}, ϕ_i and ψ_j as

$$m_{ij} = \mathcal{A}_i\mathcal{B}_j\frac{1}{p+q}e^{\xi_i+\eta_j}, \quad \phi_i = \mathcal{A}_i e^{\xi_i}, \quad \psi_j = \mathcal{B}_j e^{\eta_j}, \tag{130}$$

where

$$\mathcal{A}_i = \frac{1}{n_i!}(p\partial_p)^{n_i}, \quad \mathcal{B}_j = \frac{1}{n_j!}(q\partial_q)^{n_j}, \tag{131}$$
$$\xi_i = px_1 + p^2x_2 + p^3x_3 + \xi_{i,0}(p), \quad \eta_j = qx_1 - q^2x_2 + q^3x_3 + \eta_{j,0}(q), \tag{132}$$

$(n_1, n_2, \ldots, n_N)$ is a vector of arbitrary positive integers, p, q are arbitrary complex constants, and $\xi_{i,0}(p)$, $\eta_{j,0}(q)$ are arbitrary complex functions of p and q. It is easy to see that these m_{ij}, ϕ_i and ψ_j functions satisfy the differential Eqs. (126)–(128). Thus, the above τ function would satisfy the bilinear Eq. (125). To guarantee that this τ function is real-valued, we impose the parameter constraints

$$q = p^*, \quad \eta_{j,0}(q) = [\xi_{j,0}(p)]^*. \tag{133}$$

Under these constraints, $\eta_j = \xi_j^*$, $m^*_{n_i,n_j} = m_{n_j,n_i}$, and thus τ in (129) is real. In addition, it is easy to see that τ is the determinant of a Hermitian matrix $M = \mathrm{mat}_{1\le i,j\le N}(m_{ij})$. Furthermore, M is positive definite, since for any nonzero column vector $\mathbf{v} = (v_1, v_2, \ldots, v_N)^T$, with the superscript "$T$" representing vector transpose,

$$\begin{aligned}\mathbf{v}^{*T} M \mathbf{v} &= \sum_{i,j=1}^{N} v_i^* v_j \mathcal{A}_i \mathcal{B}_j \frac{e^{\xi_i+\eta_j}}{p+q} = \int_{-\infty}^{x_1} \sum_{i,j=1}^{N} v_i^* v_j \mathcal{A}_i \mathcal{B}_j e^{\xi_i+\eta_j} dx_1 \\ &= \int_{-\infty}^{x_1} \left| \sum_{i=1}^{N} v_i^* \mathcal{A}_i e^{\xi_i} \right|^2 dx_1 > 0. \end{aligned} \tag{134}$$

Here, we have assumed $\Re(p) > 0$ without loss of generality. Thus, τ is always positive.

Next, we need to simplify the matrix elements of this τ determinant and derive their more explicit algebraic expressions. This simplification is very similar to that we performed in Ohta and Yang (2012), Yang and Yang (2021c). By expanding $\xi_{i,0}(p)$ into a certain series containing complex parameters $\boldsymbol{a}_i = (a_{i,1}, a_{i,2}, \ldots)$ and repeating the calculations of Ohta and Yang (2012), Yang and Yang (2021c), we can show that the matrix element m_{ij} in (130) can be reduced to the expression given in Eq. (9) of Theorem 1. Since τ is positive, we can readily see that the reduced σ determinant in Theorem 1 is positive as well. Thus, the resulting solution $u = 2(\log\sigma)_{xx}$ is real-valued and nonsingular.

Regarding polynomial degrees of the determinant $\sigma(x, y, t)$, by rewriting this determinant as a larger one in Eq. (68) and performing Laplace expansion, we can readily see that its degrees in (x, y, t) are all 2ρ, with ρ given in Eq. (13).

We would like to make a comment here regarding the choice of differential operators in Eq. (131). Obviously, we can also choose more general forms of these differential operators, such as

$$\mathcal{A}_i = \frac{1}{n_i!}\left(f(p)\partial_p\right)^{n_i}, \quad \mathcal{B}_j = \frac{1}{n_j!}\left(f(q)\partial_q\right)^{n_j}, \tag{135}$$

where $f(p)$ is an arbitrary function, and the resulting τ function (129) would still satisfy the bilinear equation (125). However, such additional freedoms in the differential operators will not produce new higher-order lump solutions. To see why, we can

rewrite this $\mathcal{A}_i$ as

$$\mathcal{A}_i = \frac{1}{n_i!}\left(\frac{f(p)}{p}p\partial_p\right)^{n_i} = \sum_{k=0}^{n_i} c_{i,k}\frac{1}{(n_i-k)!}(p\partial_p)^{n_i-k}, \tag{136}$$

where $c_{i,k}$ are p-dependent complex constants. Similar treatments can be made on $\mathcal{B}_j$. These differential operators in summation form are similar to those taken in Ohta and Yang (2012). We can directly show that the m_{ij} matrix element with these differential operators of summation form can be converted to one with these differential operators as a single term in (131), after parameters $\boldsymbol{a}_i$ in the series expansion of $\xi_{j,0}(p)$ are redefined properly. Thus, no new solutions are produced.

References

Ablowitz, M.J., Clarkson, P.A.: Solitons. Nonlinear Evolution Equations and Inverse Scattering. Cambridge University Press, Cambridge (1991)

Ablowitz, M.J., Segur, H.: On the evolution of packets of water waves. J. Fluid Mech. **92**, 691–715 (1979)

Ablowitz, M.J., Villarroel, J.: Solutions to the time dependent Schrödinger and the Kadomtsev-Petviashvili equations. Phys. Rev. Lett. **78**, 570–573 (1997)

Ablowitz, M.J., Chakravarty, S., Trubatch, A.D., Villarroel, J.: A novel class of solutions of the non-stationary Schrödinger and the Kadomtsev-Petviashvili I equations. Phys. Lett. A **267**, 132–146 (2000)

Balogh, F., Bertola, M., Bothner, T.: Hankel determinant approach to generalized Vorob'ev-Yablonski polynomials and their roots. Constr. Approx. **44**, 417 (2016)

Barashenkov, I.V., Makhankov, V.G.: Soliton-like bubbles in the system of interacting bosons. Phys. Lett. A **128**, 52–56 (1988)

Bonneux, N., Dunning, C., Stevens, M.: Coefficients of Wronskian Hermite polynomials. Stud. Appl. Math. **144**, 245–288 (2020)

Buckingham, R.J., Miller, P.D.: Large-degree asymptotics of rational Painlevé-II functions: noncritical behaviour. Nonlinearity **27**, 2489 (2014)

Chang, J.H.: Asymptotic analysis of multilump solutions of the Kadomtsev-Petviashvili-I equation. Theor. Math. Phys. **195**, 676–689 (2018)

Chen, S., Grelu, P., Mihalache, D., Baronio, F.: Families of rational solution solutions of the Kadomtsev-Petviashvili I equation. Rom. Rep. Phys. **68**, 1407–1424 (2016)

Chen, J., Chen, Y., Feng, B.F., Maruno, K., Ohta, Y.: General high-order rogue waves of the (1+1)-dimensional Yajima-Oikawa system. J. Phys. Soc. Jpn. **87**, 094007 (2018)

Clarkson, P.A.: The fourth Painlevé equation and associated special polynomials. J. Math. Phys. **44**, 5350–5374 (2003)

Clarkson, P.A., Dowie, E.: Rational solutions of the Boussinesq equation and applications to rogue waves. Trans. Math. Appl. **1**, 1–26 (2017)

Clarkson, P.A., Mansfield, E.L.: The second Painlevé equation, its hierarchy and associated special polynomials. Nonlinearity **16**, R1 (2003)

Dong, J., Ling, L., Zhang, X.: Kadomtsev–Petviashvili equation: one-constraint method and lump pattern. arXiv:2108.09715 [nlin.SI] (2021)

Dubard, P., Matveev, V.B.: Multi-rogue waves solutions: from the NLS to the KP-I equation. Nonlinearity **26**, R93–R125 (2013)

Dubard, P., Gaillard, P., Klein, C., Matveev, V.B.: On multi-rogue wave solutions of the NLS equation and positon solutions of the KdV equation. Eur. Phys. J. Spec. Top. **185**, 247–258 (2010)

Felder, G., Hemery, A.D., Veselov, A.P.: Zeros of Wronskians of Hermite polynomials and Young diagrams. Physica D **241**, 2131–2137 (2012)

Fukutani, S., Okamoto, K., Umemura, H.: Special polynomials and the Hirota bilinear relations of the second and the fourth Painlevé equations. Nagoya Math. J. **159**, 179–200 (2000)

Gaillard, P.: Multiparametric families of solutions of the Kadomtsev-Petviashvili-I equation, the structure of their rational representations, and multi-rogue waves. Theor. Math. Phys. **196**, 1174–1199 (2018)
García-Ferrero, M., Gómez-Ullate, D.: Oscillation theorems for the Wronskian of an arbitrary sequence of eigenfunctions of Schrödinger's equation. Lett. Math. Phys. **105**, 551–573 (2015)
Gorshkov, K.A., Pelinovsky, D.E., Stepanyants, Yu.A.: Normal and anomalous scattering, formation and decay of bound states of two-dimensional solitons described by the Kadomtsev-Petviashvili equation. JETP **77**, 237–245 (1993)
Hirota, R.: The Direct Method in Soliton Theory. Cambridge University Press, Cambridge (2004)
Kadomtsev, B.B., Petviashvili, V.I.: On the stability of solitary waves in weakly dispersive media. Sov. Phys. Dokl. **15**, 539–541 (1970)
Kajiwara, K., Ohta, Y.: Determinant structure of the rational solutions for the Painlevé II equation. J. Math. Phys. **37**, 4693 (1996)
Lester, C., Gelash, A, Zakharov, D., Zakharov, V.E.: Lump chains in the KP-I equation. Stud. Appl. Math. (2021). https://doi.org/10.1111/sapm.12420 (see also arXiv:2102.07038)
Ma, W.X.: Lump solutions to the Kadomtsev-Petviashvili equation. Phys. Lett. A **379**, 1975–1978 (2015)
Manakov, S.V., Zakharov, V.E., Bordag, L.A., Its, A.R., Matveev, V.B.: Two-dimensional solitons of the Kadomtsev-Petviashvili equation and their interaction. Phys. Lett. A **63**, 205–206 (1977)
Novikov, S., Manakov, S.V., Pitaevskii, L.P., Zakharov, V.E.: Theory of Solitons: The Inverse Scattering Method. Plenum, New York (1984)
Oblomkov, A.A.: Monodromy-free Schrödinger operators with quadratically increasing potentials. Theor. Math. Phys. **121**, 1574–84 (1999)
Ohta, Y., Yang, J.: General high-order rogue waves and their dynamics in the nonlinear Schrödinger equation. Proc. R. Soc. A **468**, 1716 (2012)
Pelinovsky, D.: Rational solutions of the KP hierarchy and the dynamics of their poles. II. Construction of the degenerate polynomial solutions. J. Math. Phys. **39**, 5377–5395 (1998)
Pelinovsky, D.E., Stepanyants, Yu.A.: New multisoliton solutions of the Kadomtsev-Petviashvili equation. JETP Lett. **57**, 24–28 (1993)
Pelinovsky, D.E., Stepanyants, Yu.A., Kivshar, Yu.A.: Self-focusing of plane dark solitons in nonlinear defocusing media. Phys. Rev. E **51**, 5016–5026 (1995)
Petviashvili, V.I.: Equation of an extraordinary soliton. Plasma Phys. **2**, 469–472 (1976)
Rao, J., Chow, K.W., Mihalache, D., He, J.S.: Completely resonant collision of lumps and line solitons in the Kadomtsev-Petviashvili I equation. Stud. Appl. Math. (2021). https://doi.org/10.1111/sapm.12417
Satsuma, J., Ablowitz, M.J.: Two-dimensional lumps in nonlinear dispersive systems. J. Math. Phys. **20**, 1496 (1979)
Taneda, M.: Remarks on the Yablonskii-Vorob'ev polynomials. Nagoya Math. J. **159**, 87–111 (2000)
Tsuchiya, S., Dalfovo, F., Pitaevskii, L.P.: Solitons in two-dimensional Bose-Einstein condensates. Phys. Rev. A **77**, 045601 (2008)
Vorobev, A.P.: On rational solutions of the second Painlevé equation. Differ. Equ. **1**, 58 (1965)
Weiss, J.: Modified equations, rational solutions, and the Painlevé property for the Kadomtsev-Petviashvili and Hirota-Satsuma equations. J. Math. Phys. **26**, 2174 (1985)
Yablonskii, A.I.: Vesti Akad. Navuk. BSSR Ser. Fiz. Tkh. Nauk. **3**, 30 (1959). (**in Russian**)
Yang, B., Yang, J.: General rogue waves in the Boussinesq equation. J. Phys. Soc. Jpn. **89**, 024003 (2020)
Yang, B., Yang, J.: Rogue wave patterns in the nonlinear Schrodinger equation. Physica D **419**, 132850 (2021a)
Yang, B., Yang, J.: Universal rogue wave patterns associated with the Yablonskii-Vorob'ev polynomial hierarchy. Physica D **425**, 132958 (2021b)
Yang, B., Yang, J.: General rogue waves in the three-wave resonant interaction systems. IMA J. Appl. Math. **86**, 378–425 (2021c)
Zhang, Z., Li, B., Wazwaz, A., Guo, Q.: Lump molecules in fluid systems: Kadomtsev-Petviashvili I case. Phys. Lett. A **424**, 127848 (2022)